Title	Osteocyte differentiation and the formation of an interconnected cellular network in vitro
Author(s)	Mc Garrigle, M.J.; Mullen, Conleth A.; Haugh, Matthew G.; Voisin, Muriel C.; McNamara, Laoise M.
Publication Date	2016-05-26
Publication Information	Mc Garrigle, MJ,Mullen, CA,Haugh, MG,Voisin, MC,McNamara, LM (2016) 'OSTEOCYTE DIFFERENTIATION AND THE FORMATION OF AN INTERCONNECTED CELLULAR NETWORK IN VITRO'. European Cells & Materials, 31 :323-340. doi:10.22203/eCM.v031a21
Publisher	AO Research Institute Davos
Link to publisher's version	http:/dx.doi.org/10.22203/eCM.v031a21
Item record	http://hdl.handle.net/10379/6220
DOI	http://dx.doi.org/10.22203/eCM.v031a21

OSTEOCYTE DIFFERENTIATION AND THE FORMATION OF AN INTERCONNECTED CELLULAR NETWORK *IN VITRO*

M.J. Mc Garrigle[1], C.A. Mullen[1], M.G. Haugh[1], M.C. Voisin[1] and L.M. McNamara[1]*
[1] Centre for Biomechanics Research (BMEC), Biomedical Engineering, College of Engineering and Informatics, National University of Ireland, Galway

Abstract

Extracellular matrix (ECM) stiffness and cell density can regulate osteoblast differentiation in two dimensional environments. However, it is not yet known how osteoblast-osteocyte differentiation is regulated within a 3D ECM environment, akin to that existing *in vivo*. In this study we test the hypothesis that osteocyte differentiation is regulated by a 3D cell environment, ECM stiffness and cell density. We encapsulated MC3T3-E1 pre-osteoblastic cells at varied cell densities (0.25, 1 and 2 × 10^6 cells/mL) within microbial transglutaminase (mtgase) gelatin hydrogels of low (0.58 kPa) and high (1.47 kPa) matrix stiffnesses. Cellular morphology was characterised from phalloidin-FITC and 4',6-diamidino-2-phenylindole (DAPI) dilactate staining. In particular, the expression of cell dendrites, which are phenotypic of osteocyte differentiation, were identified. Immunofluorescent staining for the osteocytes specific protein DMP-1 was conducted. Biochemical analyses were performed to determine cell number, alkaline phosphatase activity and mineralisation at 2.5 hours, 3, 21 and 56 days. We found that osteocyte differentiation and the formation of an interconnected network between dendritic cells was significantly increased within low stiffness 3D matrices, compared to cells within high stiffness matrices, at high cell densities. Moreover we saw that this network was interconnected, expressed DMP-1 and also connected with osteoblast-like cells at the matrix surface. This study shows for the first time the role of the 3D physical nature of the ECM and cell density for regulating osteocyte differentiation and the formation of the osteocyte network *in vitro*. Future studies could apply this method to develop 3D tissue engineered constructs with an osteocyte network in place.

Keywords: Osteoblast, osteocyte, interconnected network, three dimensional, cell density, matrix stiffness, *in vitro.*

* Address for correspondence:
Dr. Laoise M. McNamara
Centre for Biomechanics Research (BMEC),
Biomedical Engineering,
College of Engineering and Informatics,
National University of Ireland,
Galway, Ireland,
Telephone number: (353) 91-492251
Fax number: (353) 91-563991
Email: Laoise.McNamara@nuigalway.ie

Introduction

In bone, osteocyte cells form a complex three-dimensional (3D) communication network that plays a vital role in maintaining bone health by monitoring physical cues arising during load-bearing activity and directing the activity of osteoblasts and osteoclasts to initiate bone formation and resorption (Burger and Klein-Nulend, 1999). Osteocytes are formed when cuboidal-like osteoblasts become embedded within soft secreted osteoid and start to change morphologically to a dendritic shape characteristic of an osteocyte. This transition is accompanied by a loss of cell volume (reduced organelle content) (Knothe Tate *et al*., 2004; Palumbo *et al*., 2004) and an increase in the formation and elongation of thin cytoplasmic projections that interconnect with neighbouring osteocytes within the bone ECM and osteoblasts on the surface of the bone (Palazzini *et al*., 1998; Palumbo, 1986; Mullen *et al*., 2013; Prideaux *et al*., 2012; Palumbo *et al*., 2004). Furthermore, as an osteoblast differentiates to an osteocyte, expression of the osteoblast marker enzyme alkaline phosphatase (ALP) is greatly reduced (Jee, 2001; Mikuni-Takagaki *et al*., 1995; Nakano *et al*., 2004) along with an upregulation in dentin matrix protein-1 (DMP-1) (Narayanan *et al*., 2003; Rios *et al*., 2005). During the transformation from soft secreted osteoid to a mineralised ECM, the embedded osteoblast has been shown to extend out thick cell processes that polarise towards the mineralised matrix layer. These cell processes are believed to be involved in the extrusion of calcifying matrix vesicles and hence the formation of a mineralised osteoid matrix. This is followed by the cell extending out dendrites of a longer, thinner nature towards the vascular space, which are believed to have a nutritional function (Barragan-Adjemian *et al*., 2006; Palumbo, 1986). It is believed that osteocyte cell processes play an important role in monitoring mechanical stimulation of the osteocytes, arising from fluid flow within the lacunar-canalicular network and direct mechanical strain of the bone cell membrane (Anderson and Knothe Tate, 2008; Han *et al*., 2004; Knothe Tate *et al*., 1998; Knothe Tate *et al*., 2000; Knothe Tate and Niederer, 1998; McNamara *et al*., 2009; Verbruggen *et al*., 2012; Wang *et al*., 2000; Wang *et al*., 2005; Wang *et al*., 2007; Weinbaum *et al*., 1994; You *et al*., 2001; Zeng *et al*., 1994).

Osteogenic differentiation of human mesenchymal stem cells (MSCs) and pre-osteoblasts (MC3T3-E1) has been studied on 2D surfaces (Engler *et al*., 2006; Przybylowski *et al*., 2012) and on 3D biomaterials (Correia *et al*., 2012; Curtin *et al*., 2012; Gleeson *et al*., 2010; Keogh *et al*., 2010), which act as tissue engineering (TE) scaffolds for cell attachment and tissue growth. Through these methods important cellular responses have been identified, in particular regulatory mechanisms for cell proliferation,

migration, and matrix production, which provide information that is driving the development of approaches for regenerating bone tissue *in vitro* as a treatment for large bone defects. It has been shown that substrate (2D) (Engler *et al*., 2004; Mullen *et al*., 2013) and matrix (3D) (Tan *et al*., 2014) stiffnesses are important physical factors that induce a phenotypic shift towards osteogenic differentiation. Indeed, extracellular mechanical cues are recognised as regulators of a variety of cell behaviours such as migration (Zaman and Trapani, 2006), proliferation (Hadjipanayi *et al*., 2009), and differentiation (Lo *et al*., 2000; Tan *et al*., 2014). Moreover, the extracellular mechanical environment can partially direct osteogenic differentiation and mineralisation of a variety of cells including myoblasts (Tan *et al*., 2014), osteoblasts (Chatterjee *et al*., 2010), MSCs (Engler *et al*., 2006; Huebsch *et al*., 2010; Wang *et al*., 2012) and embryonic stem cells (Evans *et al*., 2009). In particular, the effect of varying 2D substrate stiffness on cultured osteoblastic cells has been shown to favour osteocyte differentiation on relatively soft ECM substrates (0.286 kPa) (Mullen *et al*., 2013), whereas culture on a more rigid substrate (20-40 kPa) led to osteogenic differentiation (Engler *et al*., 2004).

Cell seeding density has also been shown to be a critical parameter controlling cell proliferation, ECM synthesis and osteogenic signal expression, as it dictates the paracrine signalling distance between cells (Kim *et al*., 2009; Mullen *et al*., 2013; Zhou *et al*., 2011). Using a 2D culture of pre-osteoblastic cells seeded on collagen substrates, we have recently shown that a low cell seeding density was important for dendrite formation and osteogenic differentiation, as indicated by reduced alkaline phosphatase (ALP) activity and increased mineral production (Mullen *et al*., 2013). In contrast, a high cell density resulted in the attainment of an osteoblastic phenotype, indicated by a spread morphology and high levels of ALP (Mullen *et al*., 2013).

In vivo, osteoblasts and osteocytes primarily exist within a complex three dimensional (3D) environment (Boukhechba and Balaguer, 2009), and it is known that 3D environment has a significant effect on cell morphology and geometry, as shown in NIH 3T3 fibroblast (Legant *et al*., 2010), cardiac cells (Soares *et al*., 2012) and MC3T3-E1 osteoblasts (Murshid *et al*., 2007). The process of osteocyte dendrite formation within a 3D environment is highly dynamic, as the embedding cells repeatedly extend and retract their dendrites. These "exploratory dendrites" make transient connections with already embedded osteocytes and may allow the osteocyte to position itself an appropriate spacing from other embedded osteocytes to maintain the ordered three dimensional spacing of the osteocyte network (Dallas *et al*., 2013; Zhang *et al*., 2006). However, although osteocyte differentiation has been studied in 2D (Mullen *et al*., 2013), it is not known how biophysical cues, such as matrix stiffness and cell density, control the phenotypic shift from osteoblasts to osteocytes in a 3D environment.

In this study, we test the hypothesis that osteocyte differentiation is regulated by ECM stiffness and cell density within a 3D environment. The effect of extracellular mechanical cues in a 3D environment for osteoblast-osteocyte differentiation is investigated by encapsulating MC3T3-E1 pre-osteoblastic cells homogenously within hydrogels of varying matrix stiffnesses. To investigate the effect of cell density, osteoblast cells are cultured at varying cell densities within each of the hydrogels. Osteocyte differentiation is examined by DMP-1 staining and quantifying cellular morphology, matrix mineralisation and ALP activity.

Methods

Gelatin-mtgase hydrogel preparation

Gelatin-mtgase hydrogels, with a final concentration of 3 % w/v gelatin, were prepared by mixing gelatin (type A, 175 Bloom, Sigma-Aldrich, Dublin, Ireland) at 37 °C in αMEM (Sigma-Aldrich) culture medium containing 10 % foetal bovine serum (FBS) (Sigma-Aldrich), 100 U/mL penicillin (Sigma-Aldrich), 100 g/mL streptomycin (Sigma Aldrich) and 2 mM L-glutamine (Sigma-Aldrich), to obtain a liquid consistency for easier mixing. Gelatin suspensions were sterile filtered through a 0.22 µm filter (Millipore, Cork, Ireland). Microbial transglutaminase (mtgase) (Activa WM; containing 1 % mtgase; Ajinomoto foods Europe S.A.S., Mesnil-Saint-Nicaise, France) crosslinking was carried out by mixing mtgase with the gelatin suspension, allowing to vary hydrogel stiffness by using different concentrations (0.03, 0.06, 0.08, 0.15 and 0.20 %) of mtgase *per* gram of gelatin.

Gelatin-mtgase hydrogel mechanical properties

Unconfined compression testing was used to determine the stiffness of the hydrogels exposed to different concentrations of crosslinking using a tensile tester (Z009; Zwick/Roell, Ulm, Germany) fitted with a 10 N load cell. Samples were prepared in silicon isolators (Sigma-Aldrich) that contained 8 wells of diameter 9 mm and height 2.5 mm ($n = 8$ *per* stiffness). Silicon isolators were covered with a coverslip (50 × 24 mm) (EU Thermo Scientific, Loughborough, UK) to produce a flat surface after gelation, see Fig.1. Samples were incubated in a bath of phosphate buffered saline (PBS) (Sigma-Aldrich) for 1 h at 37 °C before the coverslip and silicon isolators were removed.

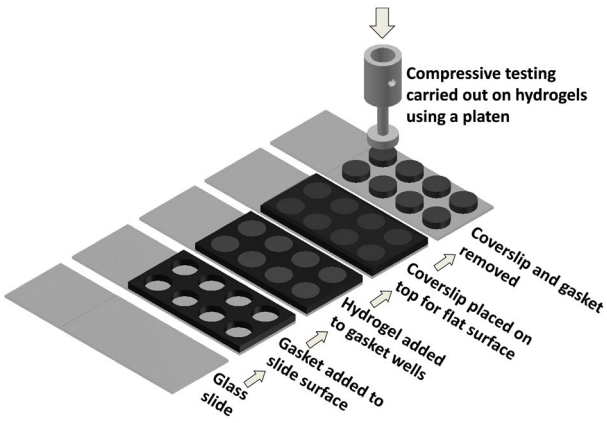

Fig. 1. Hydrogel fabrication method for mechanical testing. Unconfined compression testing was performed on samples using a custom made platen attached to a 10 N load cell.

During mechanical testing the gelatin-mtgase hydrogels were held within a bath of PBS at room temperature. Testing was conducted at a strain rate of 10 % *per* minute. The modulus was defined as the slope of a linear fit to the stress-strain curve over 2-5 % strain (Harley *et al*., 2007). Based on the results of these tests, a low and high matrix stiffness were chosen to examine the effects of 3D matrix stiffness on osteoblast differentiation and morphology.

Cell culture embedding in 3-dimensional mtgase hydrogels

MC3T3-E1 pre-osteoblastic cells (Sigma-Aldrich) were cultured under standard conditions (5 % CO_2, 37 °C). Cells were routinely grown to 70 % confluency in T175 culture flasks (Sarstedt Ltd, Wexford, Ireland) containing αMEM culture medium (Sigma-Aldrich), 10 % FBS (Sigma-Aldrich), 100 U/mL penicillin (Sigma-Aldrich), 100 g/mL streptomycin (Sigma Aldrich) and 2 mM L-glutamine (Sigma-Aldrich). Before encapsulating, MC3T3-E1 cells (Passage 15-16) were detached using trypsin-ethylenediaminetetraacetic acid (EDTA, Sigma-Aldrich) and suspended in supplemented medium at 2×10^6 cells/mL. Varying cell densities (0.25, 1 and 2×10^6 cells/mL, which is approximately 0.4, 1 and 1.6×10^4 cells/cm^2) were prepared in separate suspensions. Cell suspensions were then mixed with 6 % gelatin suspension and low and high concentrations of mtgase at a ratio of 5:4:1 (v:v:v) to give a low and high matrix stiffness. The final concentration of the mixture was 3 % w/v gelatin, (0.25, 1 and 2×10^6 cells/mL) within mtgase concentrations of 0.03 % and 0.08 % *per* gram of gelatin. Hydrogel suspensions for biochemical assays and morphology analysis were aliquoted into 96-well plates at 0.071 mL/well. All hydrogels had a height of 2 mm and were allowed to gel at 4 °C for 6 min before medium was added.

DNA content

DNA content was evaluated using the Hoechst 33258 DNA assay, which fluorescently labels double-stranded DNA (Sigma-Aldrich), as previously described (Haugh *et al*., 2011). After 2.5 h, 3, 21 and 56 d of incubation, cell laden hydrogels were washed twice with PBS, frozen and stored at −80 °C. Samples were then thawed and digested overnight in papain digest (100 mM sodium phosphate buffer containing 10 mM L-cysteine, 125 µg/mL papain and 5 mM Na_2EDTA (all from Sigma Aldrich) in ddH_2O at pH 6.5 and 60 °C). Once the samples were digested, the biochemical assays were performed straight away or stored at −80 °C until the assays could be performed. Briefly, 200 µL of Hoechst dye solution was added to 20 µL of digested samples / standards in a 96-well plate in triplicate. Fluorescence was then measured (excitation: 355 nm; emission: 460 nm) using a fluorescence spectrophotometer (Synergy HT Multi-mode microplate reader). Readings were converted to DNA content using a standard curve, according to the manufacturer's protocol, with samples containing no cells subtracted as background.

Morphological analysis of cell phenotype

Hydrogel constructs were fixed using 4 % (w/v) paraformaldehyde (Sigma-Aldrich) after 2.5 h, 21 and 56 d of culture, for 1 h under rotation. Cells within the hydrogels were permeabilised with 2 mM sodium chloride (NaCl), 1.5 mM magnesium chloride ($MgCl_2$), 16 mM sucrose and 0.5 % Triton-X100 in PBS (all from Sigma-Aldrich) for 10 min at 4 °C under rotation and washed with 1 % PBS three times. Hydrogels were then stained with phalloidin-fluorescein isothiocyanate (phalloidin-FITC) solution at 1.25 µg/mL (diluted 1:400, Sigma Aldrich) to stain the actin cytoskeleton and DAPI dilactate (diluted 1:2000, Sigma Aldrich) to stain the nucleus and rinsed again with 1 % PBS solution. Confocal scans were taken using a confocal microscope (Olympus Fluoview FV1000) at magnifications of 10 × for the hydrogel surface, 20 × and 40 × for cells below the hydrogel surface.

Maximum intensity images were generated from z-stacks taken at 20 × magnification with a distance of 5 µm between each slice for a thickness of 25 µm, while 40 × magnification z-stacks were taken at a distance of 2.5 µm between each slice for a thickness of 10 µm. All stacks were obtained at the same distance of 50 µm below the hydrogel surface. In total 15 stacks were obtained at each time-point, for each condition (five on each replicate hydrogel).

Cell processes were defined as cellular features composed of actin, located at the cell membrane, which extended for a distance of at least 10 µm from the cell body, as previously described (Mullen *et al*., 2014). Cells at later time-points, day 21 and 56 that retained a strong fluorescent actin cytoskeleton and also maintained a cell body were classified as "active", while cells that demonstrated a balled up and encapsulated morphology with a cell diameter less than 15 µm were classified as "dormant". Using this classification method cell morphologies were quantified as follows: (1) "dendritic" cells exhibited the small cell body and long thin cell processes associated with osteocytes, (2) "spherical" cells had no cell processes and exhibited a spherical or cuboidal morphology, (3) "dendritic interconnected" cells represented the number of cell process that formed interconnections with neighbouring cell processes and (4) "dividing" cells represented splitting cells within the hydrogel that remain connected. Cell morphology was quantified using NIH ImageJ software particle analysis. After 2.5 h and 21 d average cell span was determined from the diameter of the dendritic cell. By day 56, individual dendrites were manually measured and average dendrite length was determined.

Live cell imaging to track exploratory dendrites

During the 56 d culture period live cell images of the same location within hydrogels were taken at 20 × magnification using an Olympus IX50 inverted brightfield microscope. The same cell locations were identified by scoring the bottom of 96-well plates with a grid, indicating the x and y coordinate, and through focusing within the z plane to identity the same cells. Images were taken every 3-4 d.

DMP-1 immunofluorescent staining

DMP-1 is a secreted protein that is upregulated during osteoblast to osteocyte differentiation and has been observed in late stage osteoblast (D'Souza *et al*., 1997; Feng *et al*., 2002) and early stage osteocytes (Dallas and

Bonewald, 2010; Lee *et al*., 2014; Narayanan *et al*., 2003; Rios *et al*., 2005). Immunofluorescent staining for DMP-1 was conducted to investigate the phenotypic differentiation of MC3T3-E1 cells.

Hydrogel constructs were fixed using 4 % paraformaldehyde (Sigma-Aldrich) after 21 and 56 d of culture for 1 h under rotation. Cells within the hydrogels were permeabilised with 2 mM sodium chloride (NaCl), 1.5 mM magnesium chloride ($MgCl_2$), 16 mM Sucrose and 0.5 % Triton-X100 in PBS (all from Sigma-Aldrich) for 10 min at 4 °C under rotation and washed in PBS 3 times. Hydrogel constructs were covered with a 10 % bovine serum albumin (BSA) / 3 % normal goat serum (NGS) (Jackson Immunoresearch) blocking solution for 1 h under rotation before incubation with monoclonal anti-DMP1 antibody at a dilution of 1:100 at 4 °C overnight (Clone 8G10.3, Millipore). After washing 3 times with 1 %BSA/PBS solution, samples were then treated with a Dylight™ 549 conjugate goat anti-mouse secondary antibody at a dilution of 1:100 (Jackson Immunoresearch) for 1 h under rotation at room temperature. After secondary staining, samples were rinsed 3 times with 1 % BSA/PBS solution. Hydrogels were then further counterstained with phalloidin-FITC at 1.25 µg/mL (diluted 1:400, Sigma Aldrich) to stain the actin cytoskeleton and DAPI dilactate (diluted 1:2000, Sigma Aldrich) to stain the nucleus and rinsed again with 1 % BSA/PBS solution. Confocal scans were taken using a confocal microscope (Olympus fluoview) at 10 × and 40 × magnification. Z-stacks were combined together in 2D to form maximum intensity images. Negative controls were performed by omitting the primary antibody incubation step.

Extracellular ALP content

Extracellular alkaline phosphatase (ALP) activity was determined using a colorimetric assay of enzyme activity (SIGMAFAST *p*-NPP Kit, Sigma Aldrich), which uses *p*-nitrophenyl phosphate (*p*NPP) (nmol) as a phosphatase substrate, with ALP enzyme (Sigma Aldrich) as a standard. Prior to medium change, medium was removed from samples at each time-point and frozen and stored at −80 °C, 40 µL of the medium was added to a 96-well plate in triplicate with a 50 µL of *p*NPP solution, which contains both *p*NPP and assay buffer. The samples were shielded from direct light at room temperature for 1 h. After this, 20 µL of Stop Solution (3 M NaOH) was added to the wells and the plate was read at 405 nm in a Synergy HT Multi-mode microplate reader. Results were then normalised to cell number (µg) as determined through the Hoescht assay outlined above and expressed as nmol/µg.

Mineralisation

Mineralisation within hydrogel constructs was determined from calcium deposition and measured using the Calcium Liquicolour kit (Stanbio Laboratories, Syntec, Dublin, Ireland) according to the manufacturer's protocol. After 21 and 56 d of incubation, cell laden hydrogels were washed twice with PBS, frozen and stored at −80 °C. Hydrogel samples were then thawed and digested by adding 16.6 µL of 6 M hydrochloric acid (HCL) (Sigma-Aldrich) to each well and storing the solution at 4 °C, when completely dissolved HCL concentration was adjusted to 0.5 M HCL by adding 183.4 µL of ddH_2O to each sample. 10 µL each of the digested samples and assay standard was added to a 96-well plate and 200 µL of the working solution. The plate was read on a synergy HT Multi-mode microplate reader at an absorbance of 550 nm as previously described.

Statistics

All biochemical experiments were conducted in biological triplicate with two independent experiments run for a total of $n = 6$. Cell morphology experiments were conducted in duplicate with two independent experiments run for a total of $n = 4$. Results are expressed as mean ± standard deviation. For all the biochemical analysis two-way analysis of variance (ANOVA) was conducted, followed by pair-wise multiple comparison procedure (Tukey's HSD test). All analyses were performed with Graphpad Prism 6 (GraphPad software, San Diego, USA). For all comparisons, the level of significance was $p \leq 0.05$.

Results

Compressive modulus

Compressive testing of varied stiffness of hydrogels showed an increase in stiffness with varied cross-linking concentration after incubation for 1 h at 37 °C, see Fig. 2. Mtgase hydrogels containing 0.03, 0.06, 0.08, 0.15, 0.2 % mtgase had compressive moduli of 0.58 ± 0.1, 0.84 ± 0.1, 1.47 ± 0.3, 3.05 ± 0.2 and 3.03 ± 0.4 kPa respectively. The effect of increasing cross-linking density on hydrogel stiffness reached a plateau at 0.15 % mtgase crosslinking. We sought to encapsulate cells in a similar mechanical environment to our previous studies using 2D substrates (~ 0.3 kPa), which were shown to elicit osteoblast-osteocyte differentiation (Mullen *et al*., 2013). The compressive moduli 0.58 kPa was the lowest achievable stiffness in this 3D environment, while a higher matrix stiffness (1.47 kPa) was selected from the gels that were crosslinked at different densities, see Fig. 2, on the basis that it was statistically significantly higher matrix stiffness (1.47 kPa) compared to the low matrix stiffness.

DNA content

DNA content increased significantly in all matrix stiffness and cell density groups from 2.5 h to 56 d of culture ($p < 0.0001$), see Fig. 3. By day 56 in the medium cell density group (1×10^6 cells/mL) a significant difference was observed between the low and high matrix stiffness (3.28 ± 1.02 µg *vs.* 2.53 ± 0.55 µg, $p < 0.03$).

Morphological analysis of cell phenotype

MC3T3-E1 morphology and dendritic cell span after 2.5 h

MC3T3-E1 cells cultured at low and medium cell densities within low stiffness matrices (0.58 kPa) showed a similar morphological pattern with approximately 81.5 % classed as spherical and 18.5 % as having a dendritic morphology after 2.5 h ($p < 0.0001$). However, cells cultured within a high stiffness matrix (1.47 kPa) at a low and medium cell density were classified as being approximately 99 % spherical and 1 % dendritic ($p < 0.0001$). In the

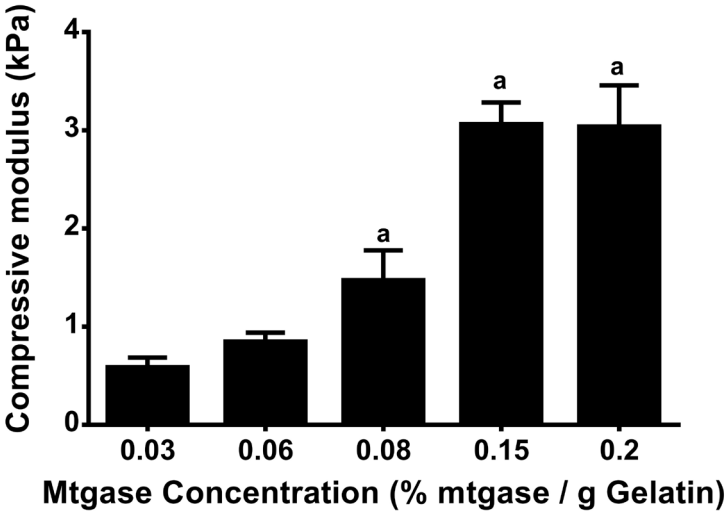

Fig. 2. Mechanical properties of a 3 % Gelatin hydrogel crosslinked with 0.15, 0.03, 0.06, 0.08, 0.15, 0.2 % mtgase after 1 h of incubation at 37 °C, n = 8 *per* group. $^{a}p < 0.05$ relative to 0.03 % mtgase hydrogel.

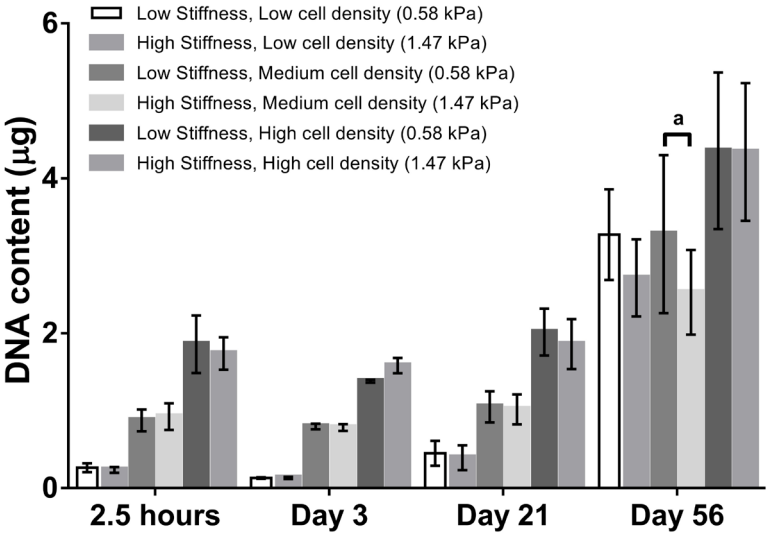

Fig. 3. DNA content of each group at 2.5 h, 3, 21 and 56 d (n = 6 samples *per* group *per* time-point). $^{a}p < 0.05$ representing a statistical difference between low (0.58 kPa) and high (1.47 kPa) stiffness. Error bars denote standard deviation.

high cell density groups, within a low stiffness hydrogel (0.58 kPa), cells were classed to be 71.5 % spherical and 28.5 % dendritic ($p < 0.0001$). In contrast, cells within the high stiffness matrices were classed as 97 % spherical and 3 % dendritic ($p < 0.0001$). Furthermore, for all cell density groups a larger percentage of dendritic cells were observed in the low stiffness matrices compared to the higher stiffness ($p < 0.0012$), see Fig. 4**A** for representative images and Fig. 4**B** for summarised results.

After 2.5 h, dendritic cell span in the low stiffness matrices within each cell density had similar cell span lengths, though not significantly different, 58 µm in the low cell density, 56 µm in the medium cell density and 64 µm in the high cell density, while no change occurred in the higher matrix stiffness hydrogels remaining at approximately 24 µm, see Fig. 4**C**.

MC3T3-E1 morphology and dendritic cell span after 21 d
For a low cell density and a low stiffness matrix, 52 % of the cells were classified as spherical, while 48 % of cells were dendritic after 21 d. In contrast, for a high stiffness matrix, 82.6 % of cells were spherical, while 17.4 % of cells were dendritic ($p < 0.0001$). Cells cultured at medium and high cell densities within a low stiffness matrix showed a similar morphological pattern with approximately 24 % classed as spherical and 76 % as dendritic morphology for both seeding densities ($p < 0.0005$). In contrast within the high stiffness matrix, at a medium and high cell density, approximately 94 % cells were spherical and 6 % dendritic ($p < 0.0001$). Additionally, all cell density groups showed a significant increase in the percentage of dendritic cells in the low stiffness matrices compared to the high stiffness ($p < 0.0386$), see Fig. 5**A** for representative images and Fig. 5**B** for summarised results.

Dendritic cell span in the low stiffness matrices showed a trend of increasing as cell density increased though not significantly different. Specifically the cell span was 60.1 µm in the low cell density, 67.7 µm in the medium cell density and 82.2 µm in the high cell density. A smaller change occurred in higher stiffness matrices, 46.7 µm in the

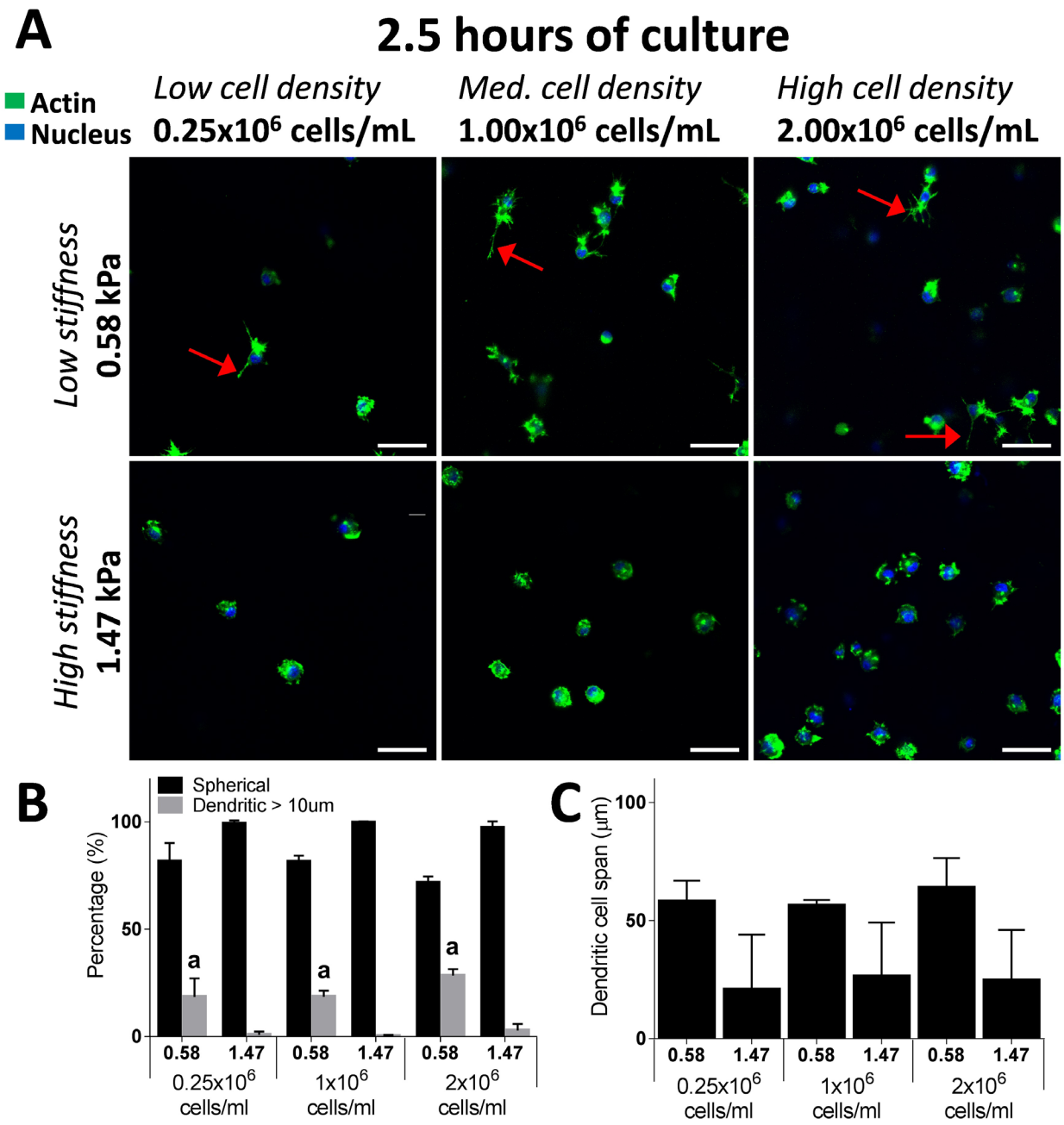

Fig. 4. Actin staining of cell morphology after 2.5 h of culture comparing spherical *vs*. dendritic (Red arrows) morphology (**A**). Also shown is the percentage of spherical *vs*. dendritic cells (**B**) and average dendritic cell span (**C**) within low (0.58 kPa) and high (1.47 kPa) stiffness matrices. $^{a}p < 0.05$ representing a statistical difference between low (0.58 kPa) and high (1.47 kPa) stiffness at the same density group. Scale bar = 50 µm, same for all images.

low cell density, 50.3 µm in the medium cell density and 56.4 µm in the high cell density, though not significantly different. A significant difference was observed between the low and high matrix stiffness at the high cell density group ($p < 0.0491$), see Fig. 5**C**.

MC3T3-E1 morphology, dendritic cell length and interconnections after 56 d

By 56 d, in all hydrogel groups, cells formed a confluent layer at the surface of the hydrogels, see Fig. 6 and Fig. 7. Below the surface, at low and medium cell densities within a low stiffness matrix, cells showed similar morphology patterns with approximately 24 % spherical and 76 % dendritic ($p < 0.0001$). However, cells cultured within a high stiffness matrix at a low and medium cell density were classified to be approximately 60 % spherical and 40 % dendritic, though not significantly different. For a high cell density and a low stiffness matrix, 14.6 % were classed as spherical, while 85.4 % were dendritic ($p < 0.0001$). In contrast, cells within a high stiffness matrix were 64.6 % spherical and 34.4 % dendritic ($p < 0.0148$). Similarly to day 21, a larger percentage of dendritic cells were observed in the low stiffness matrices compared to the high stiffness in all cell density groups ($p < 0.0093$), see Fig. 8**A** for representative images and Fig. 8**B** for summarised results.

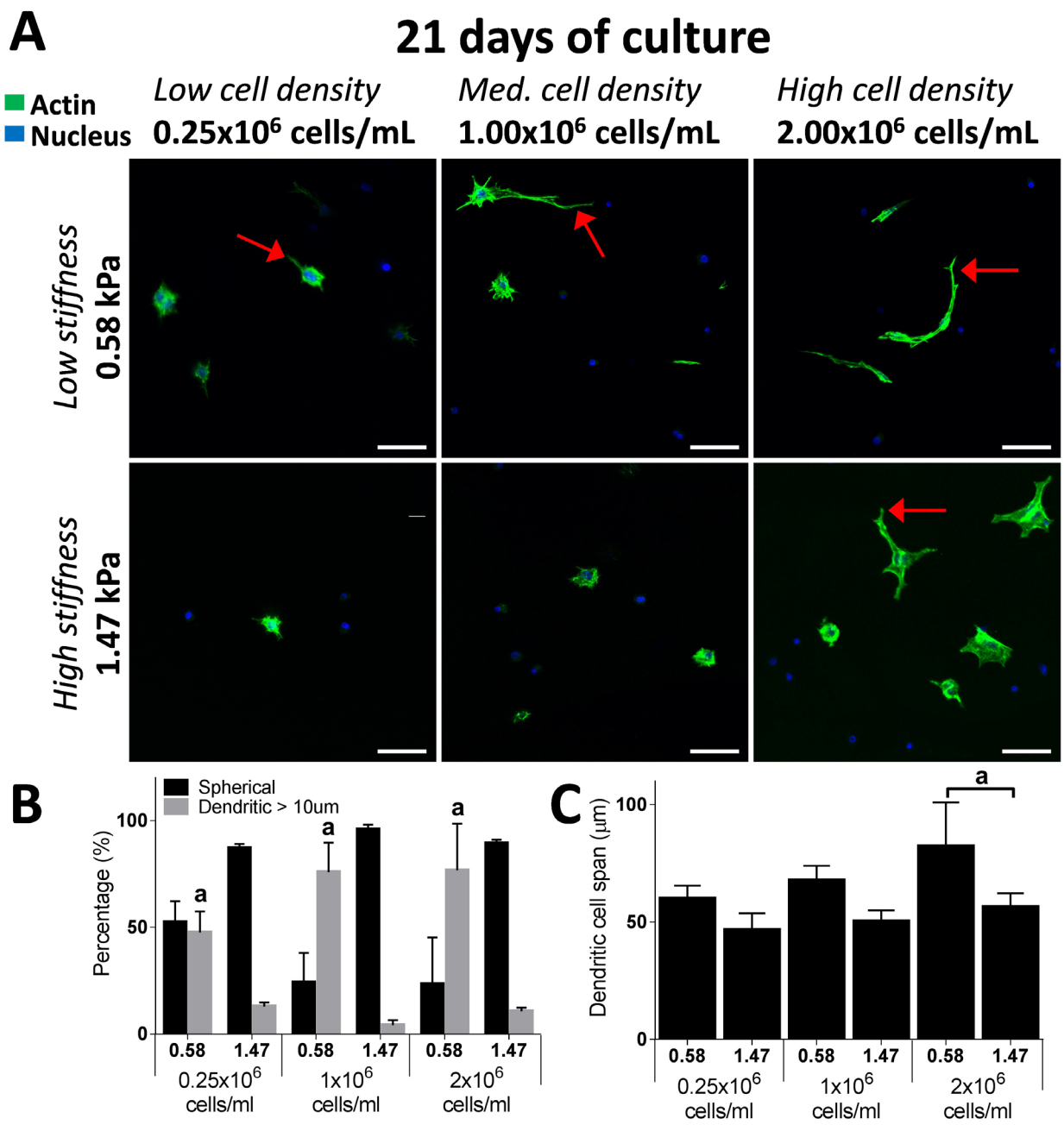

Fig. 5. Actin staining of cell morphology after 21 h of culture comparing spherical *vs*. dendritic (Red arrows) morphology (**A**). Also shown is the percentage of spherical *vs*. dendritic cells (**B**) and average dendritic cell span (**C**) within low (0.58 kPa) and high (1.47 kPa) stiffness matrices. [a]$p < 0.05$ representing a statistical difference between low (0.58 kPa) and high (1.47 kPa) stiffness at the same density group. Scale bar = 50 µm, same for all images.

At 56 d, average individual dendrite length within the low stiffness matrices was 46.2 µm in the low cell density, 53.9 µm in the medium cell density and 67.2 µm in the high cell density. Dendrite length in higher stiffness matrices was 35.7 µm in the low cell density, 36.9 µm in the medium cell density and 29.3 µm in the high cell density. Furthermore, a significant difference was observed between the low and high matrix stiffness at the high cell density group ($p < 0.0095$), see Fig. 8**C**.

Cell interconnections after 56 d

Cells at a high cell density within a low stiffness matrix had the highest number of interconnections between neighbouring dendritic cells compared to the high stiffness matrix at the same density ($p < 0.037$). Cells were classified as 38.8 % interconnected, whereas 30.9 % were unconnected and 30.3 % connected as dividing cells. For the higher stiffness matrix at the same cell density 4.6 % of cells were interconnected, 89.1 % were unconnected and 6.3 % connected as dividing cells. At a medium cell density, within a low stiffness matrix, cells were approximately classified as 16.5 % interconnected, while 32 % were unconnected and 51.5 % connected as dividing cells. For the higher stiffness matrix at the same cell density 2.8 % of cells were interconnected, 71.9 % were unconnected and 25.3 % connected as dividing

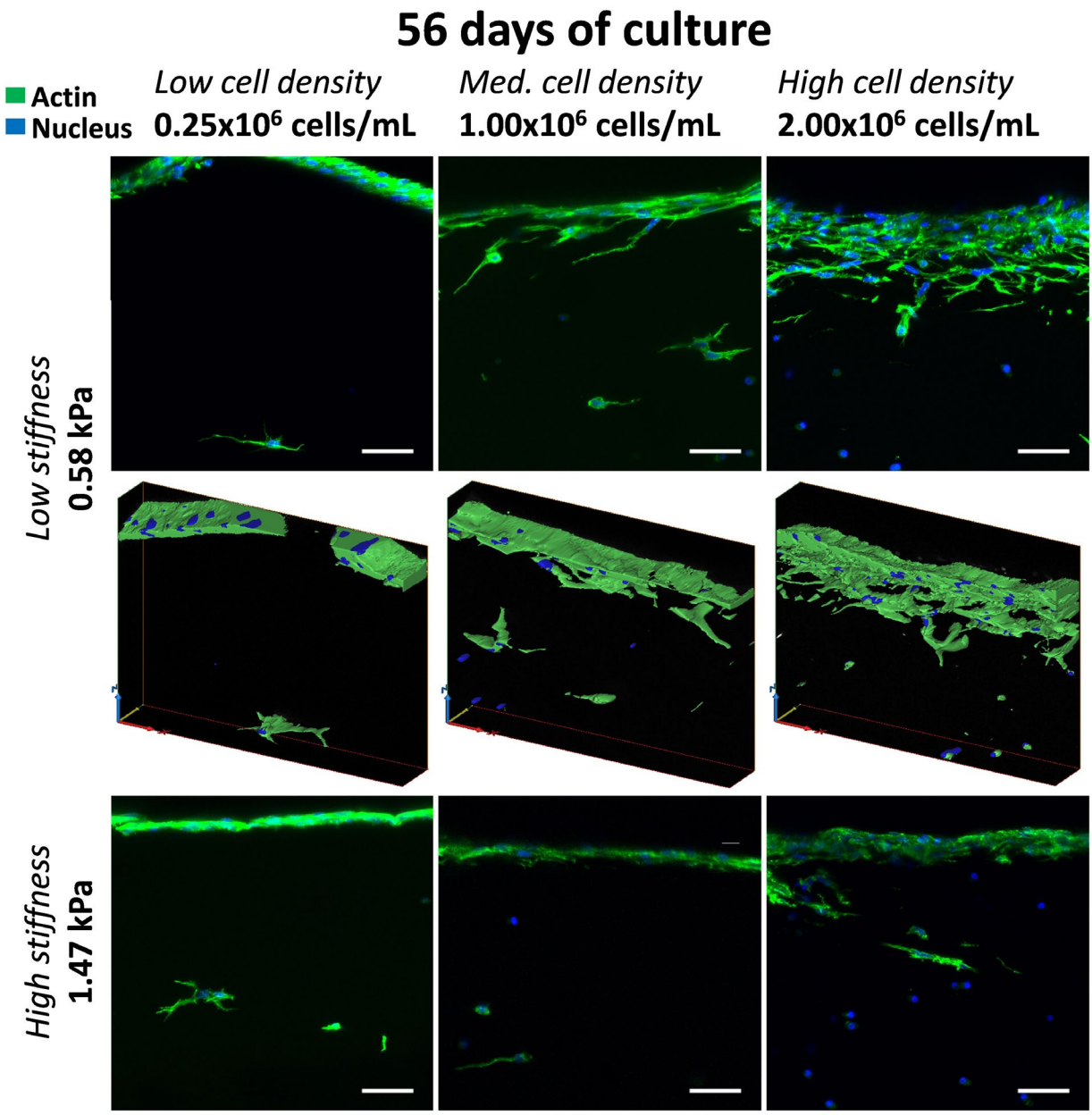

Fig. 6. Section views of cell morphologies and interconnections at 56 d. Fluorescent images represented as 3D stacks in low stiffness matrix group. Scale bar = 50 µm.

cells. For the low cell density within a low stiffness matrix 6.9 % of cells were interconnected, while 36.5 % were unconnected and 56.6 % connected as dividing cells. For the higher stiffness matrix at the same cell density 4.6 % of cells were interconnected, 89.1 % were unconnected and 6.3 % connected as dividing cells, see Fig. 8**D**.

Exploratory dendrites live cell imaging

Cell dendrite formation was observed after 1 h of incubation within the lowest stiffness hydrogel. Dendrite formation was observed to increase with time. Dendrites were observed to be highly dynamic as cells repeatedly formed interconnections, extended and retracted their dendrites over the culture period. It was also observed that individual cells were active and viable throughout the entire 56 d culture period without proliferating, see Fig. 9**A**, 9**B**. However, it was also observed that an individual cell that initially exhibited a dendritic morphology, could became balled up, reduce in size and remain in the hydrogel for the 56 day culture period (Fig. 9**A**, black arrows). These cells were referred to as "dormant" due to showing no normal cell activity (dendritic, motile, change in cell morphology, *etc.)* throughout the culture period.

DMP-1 immunofluorescent staining

Immunofluorescent staining for DMP-1 showed positive expression of DMP-1 within the proximity of cells encapsulated within the soft stiffness matrix (0.58 kPa), see Fig. 10. At 10 × magnification, DMP-1 staining was observed within the proximity of dendritic and interconnected cells at a medium cell density, see Fig. 10**B**. At 40 × magnification, at a low and high cell density, DMP-

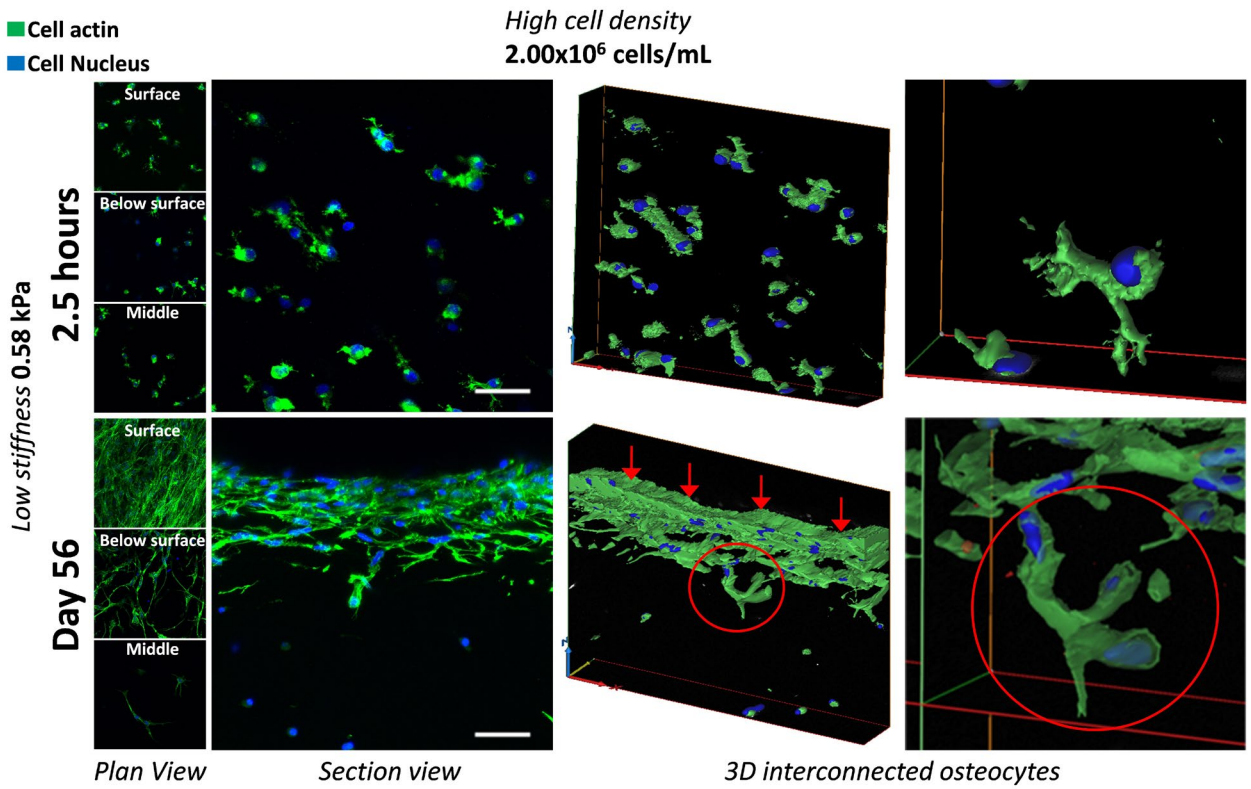

Fig. 7. Section view images of low stiffness matrix and high cell density comparing cell morphologies and interconnections at 2.5 h and 56 d. After 2.5 h, cells form dendrites throughout the hydrogel. By 56 d, cells proliferate on surface, exhibiting a spread and confluent morphology (red arrows), progressing from the hydrogel surface cells become dendritic and forming interconnections (red circle). Scale bar = 50 µm.

1 staining was observed within matrices at day 21 and 56 (Fig. 10**C**-**F**). DMP-1 staining, at the high cell density was observed as dispersed nodules within the surrounding matrix of dendritic and interconnected cells (blue arrows) (Fig. 10**E**, 10**F**). DMP-1 staining was not observed in the negative control, where the primary antibody was omitted (Fig. 10**A**).

ALP activity of cells

Extracellular alkaline phosphatase activity by day 3 showed a significant increase for the low cell density group within both the low and high stiffness matrices compared to all other groups at the same time-point ($p < 0.0001$). Furthermore, at a low cell density a significant increase in ALP activity was also observed in the high stiffness matrix compared to the low stiffness matrices (15.18 ± 2.1 nmol/µg *vs.* 12.31 ± 1.22 nmol/µg, $p < 0.0002$). Similarly, by day 21 significantly higher ALP activity was observed within the low cell density groups for both the low and high stiffness matrices compared to the other groups at the same time-point ($p < 0.0002$). By day 56, ALP activity was downregulated in all groups with no significant difference between groups, see Fig. 11.

Mineralisation

Calcium content in the high cell density group within a low and high stiffness matrix showed a significant increase in mineralisation from day 21 to 56 ($p < 0.05$). By day 56, significantly higher calcium content was observed in the high cell density group within both the low and high stiffness matrix compared to the other groups at the same time-point ($p < 0.05$). Furthermore, a significant difference ($p < 0.0287$) in calcium content was observed between the low and high matrix stiffness (29.23 ± 7.38 µg 20.3 ± 10.06 µg), see Fig. 12.

Discussion

The results of this study show for the first time that osteocyte differentiation of MC3T3-E1 cells is regulated within a 3D cell environment by ECM stiffness and cell density. Specifically, we showed that the highest extent of osteoblast-osteocyte differentiation occurred within a soft 3D matrix (0.58 kPa) at high cell density (2×10^6 cells/mL). Interestingly, after 56 d of culture these conditions led to the formation of an osteocyte-like network within the 3D matrix, characterised by long dendrites interconnecting with neighbouring osteocytic cells. DMP-1, a secreted protein that is upregulated during osteoblast to osteocyte differentiation, was identified within the matrix by immunohistochemistry. At the surface of this matrix cells formed a confluent layer, characteristic of osteoblast-like cells, which was also interconnected with the osteocyte-like network. Bone has a similar structure *in vivo*, wherein osteocytes form a complex interconnected network allowing for communicating with their neighbours and with osteoblasts cells on bone surfaces *via* long cellular

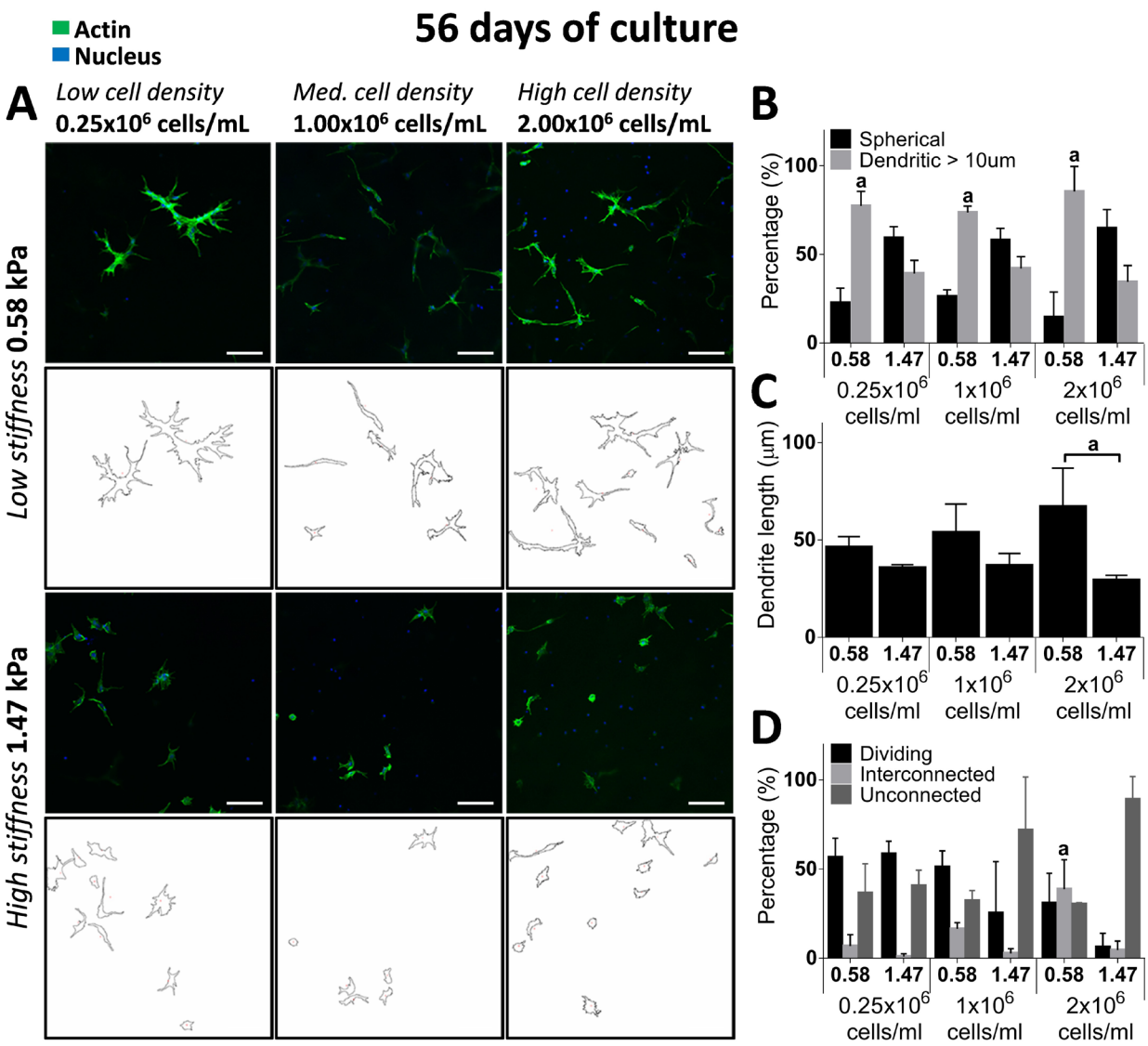

Fig. 8. Actin staining and particle analysis illustrations of cell morphology after 56 d of culture comparing spherical *vs*. dendritic morphology (**A**) within low (0.58 kPa) and high (1.47 kPa) stiffness matrices. Also shown is the percentage of spherical *vs*. dendritic cells (**B**), average cell dendrite length (**C**) and percentage of interconnections formed between cells (**D**). $^{a}p < 0.05$ representing a statistical difference between low (0.58 kPa) and high (1.47 kPa) stiffness at the same density group. Scale bar = 100 µm.

processes. Within a stiffer matrix (1.47 kPa) at a low cell density, dendrite formation occurred but these dendrites were shorter and a reduced interconnecting network was established. These findings reveal that both the mechanical properties of ECM and the ability for cells to establish a communication network within a 3D environment, play a significant role in osteocyte differentiation and the formation an interconnected network.

Cell migration, proliferation and differentiation have all been shown to be influenced by substrate (2D) or matrix (3D) stiffness (Engler *et al*., 2004; Hadjipanayi *et al*., 2009; Lo *et al.,* 2000; Mullen *et al*., 2013; Tan *et al*., 2014; Zaman and Trapani, 2006). In particular, a soft 2D substrate (0.3 kPa) was shown to lead to osteocyte differentiation (Mullen *et al*., 2013), whereas more rigid 2D substrates (40 kPa) favour osteoblast differentiation (Engler *et al*., 2004). Osteoblast to osteocyte differentiation has been previously elicited in human primary osteoblast-like cells within 3D collagen gels, with 10 % of cells becoming dendritic and expressing osteocyte-specific gene E11 after 28 d (Atkins *et al*., 2009). Primary mouse calvarial and MC3T3-E1 cells formed dendrites and expressed osteocyte-specific genes (DMP1, Sost, Phex) after 35 d on type I collagen gels with osteogenic supplements (β-glycerophosphate and ascorbic acid) (Uchihashi *et al*., 2013). The mouse clonal cell line (IDG-SW3) developed dendrites and expressed osteocytic markers (DMP1, Sost) after 30 d on 3D collagen sponges (Woo *et al*., 2011). Osteoblast-osteocyte differentiation, has been induced in human osteoblasts cultured in 3D with hydroxyapatite/tricalcium phosphate biphasic calcium phosphate ceramic particles (Boukhechba and Balaguer, 2009). However, these

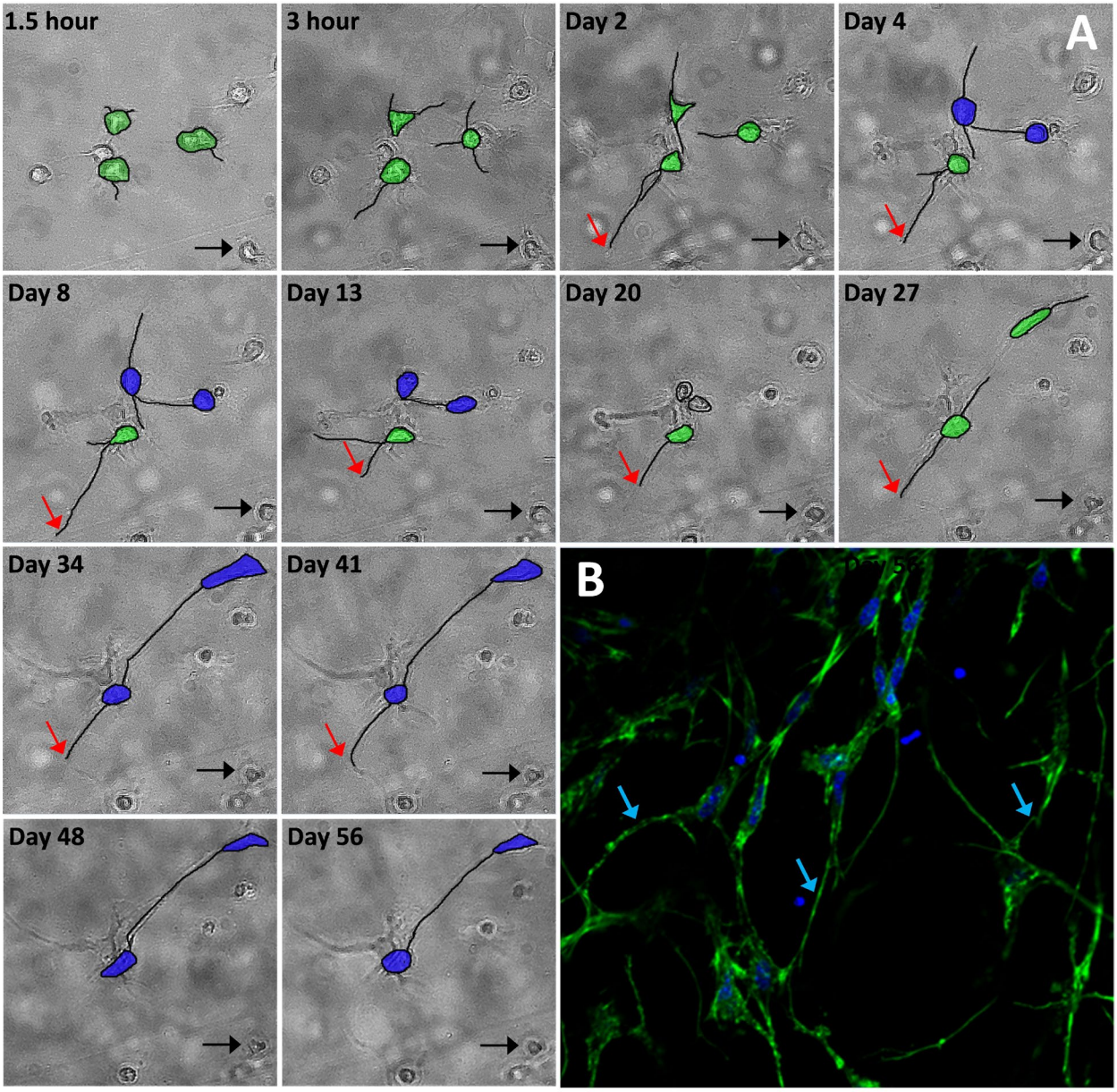

Fig. 9. (**A**) Live cell imaging of a low stiffness matrix at a high cell density show cells (green cells) to be highly dynamic and constantly sending out exploratory dendrites (red arrow) throughout the study, while at the later time-points the same cells formed interconnections with neighbouring cells (blue cells). Furthermore, cells that became balled up and encapsulated (Black arrows), were observed to remain balled up within the hydrogel throughout the 56 d culture period and were classified as dormant. (**B**) Fluorescent imaging at day 56 show interconnections formed between cells (blue arrow).

studies did not characterise the mechanical properties of the 3D matrix and could not uncover the role of the mechanical environment for eliciting osteocyte differentiation. The hydrogel stiffness used here (0.58/1.47 kPa) are within the range of gelatin-mtgase hydrogels (1.58/32.32 kPa) used to elicit differentiaton of mouse myoblast cells towards osteoblasts (Tan *et al*., 2014), which showed osteoblast-like cells became elongated at stiffnesses of 1.58 kPa, but were spherical at higher stiffnesses (32.32 kPa) (Tan *et al*., 2014). In the current study we show for the first time that osteocyte differentiation and the formation of interconnections is governed by soft 3D matrices (0.58 kPa). In contrast to previous studies, these results were achieved without addition of osteogenic growth factors.

In vivo, osteocytes are formed when osteoblasts become embedded within soft secreted osteoid and undergo a dramatic phenotypic transition to a dendritic shape (Knothe Tate *et al*., 2004; Palumbo *et al*., 2004), secrete DMP-1 protein, and form interconnections with neighbouring and surface cells to establish the osteocyte network. Interestingly, we observed the same traits of a dramatic phenotypic transition to a dendritic shape, DMP-1 expression and formation of an osteocyte network in cells cultured within a soft matrix. We propose that the

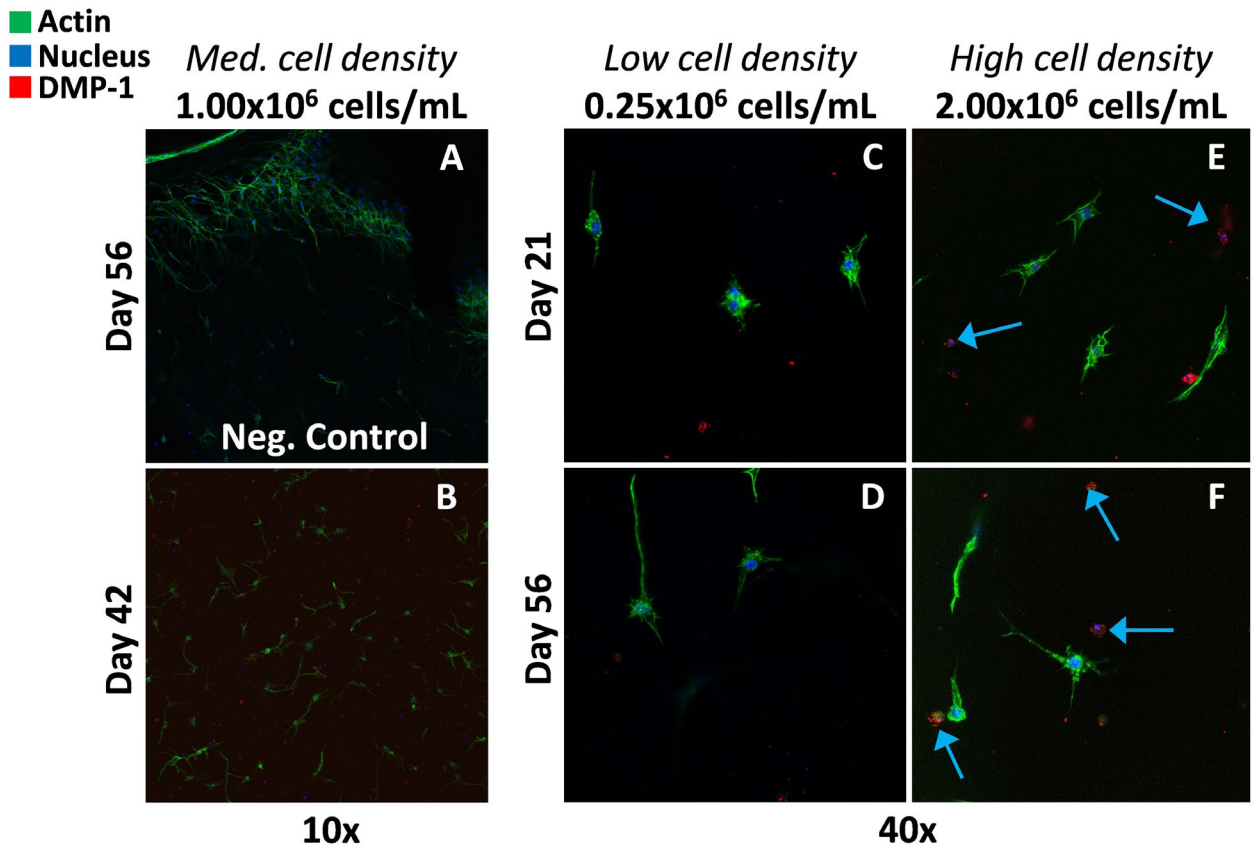

Fig. 10. Immunofluorescent images of DMP-1 from cells encapsulated in a hydrogel at a low matrix stiffness (0.58 kPa). (**A**) Negative controls were performed by omitting the primary antibody and no DMP-1 staining was observed. (**B**) DMP-1 staining was observed within the proximity of dendritic and interconnected cells at a medium cell density (10 × magnification). At a low (**C**, **D**) and high (**E**, **F**) cell density, DMP-1 staining was observed within matrices at day 21 and 56 (40 × magnification). DMP-1 staining, at the high cell density (**E**, **F**) was observed as dispersed nodules within the surrounding matrix of dendritic and interconnected cells (Blue arrows, 40 × magnification). Images were taken at approximately 50 µm below the hydrogel surface. Scale bar for 10 × (**A**, **B**) = 120 µm; 40 × (**C**, **D**, **E**, **F**) = 50 µm.

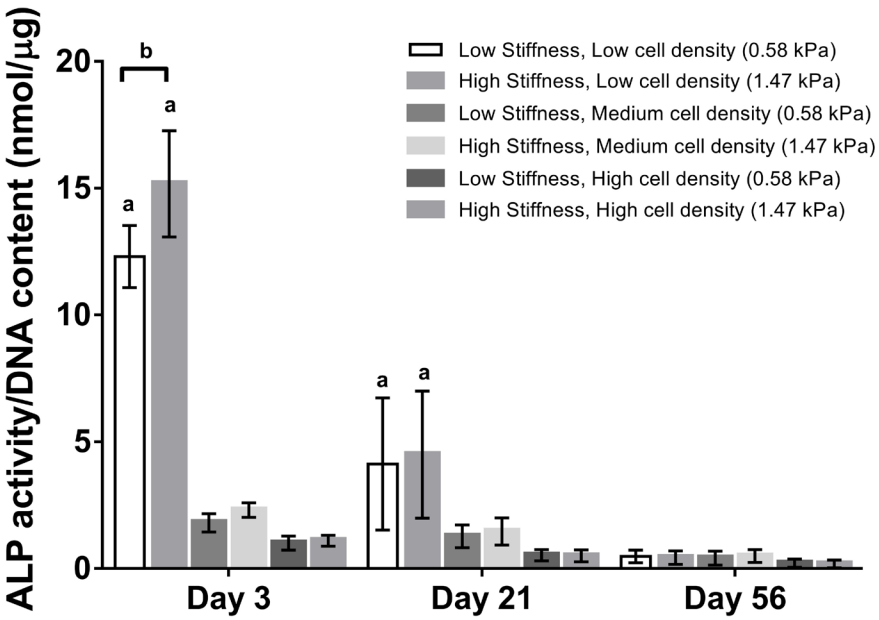

Fig. 11. Extracellular ALP activity of each group at day 3, 21 and 56 (n = 6 samples *per* group *per* time-point). $^{a}p < 0.05$ relative to the other cell density groups at the same time-point and $^{b}p < 0.05$ representing a statistical difference between low and high stiffness. Error bars denote standard deviation.

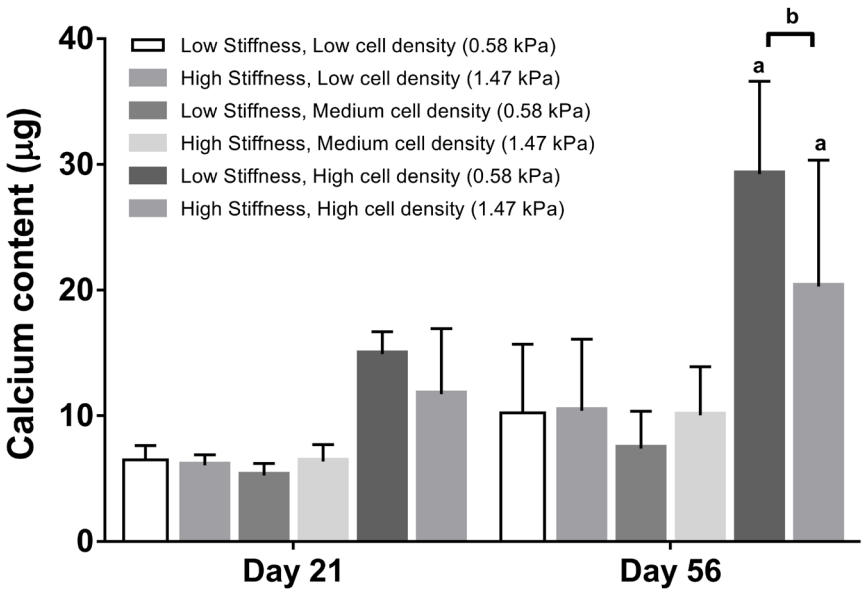

Fig. 12. Calcium content of each group at days 21 and 56 (n = 6 samples *per* group *per* time-point). [a]$p < 0.05$ relative to the other cell density groups at the same time-point. [b]$p < 0.05$ relative to the other matrix stiffness groups at the same time-point. Error bars denote standard deviation.

mechanical properties of the hydrogel matrix might provide similar extracellular mechanical cues to that of osteoid, which is a crucial component required for the embedding of an osteoblast and stimulating osteocyte differentiation *in vivo*.

Previous *in vitro* studies have shown the significance of cell density on osteogenic cell differentiation. Rat bone marrow stromal cells (BMSC) grown at low density (7.5×10^4 cells/cm^2) for 8 d on 2D poly(propylene fumarate), expressed higher amounts of ALP activity compared to cells at a high density (14.9×10^4 cells/cm^2) (Kim *et al*., 2009). We previously reported that MC3T3-E1 cells cultured at low density (0.1×10^4 cells/cm^2) had higher ALP activity compared to those at high density (1×10^4 cells/cm^2), albeit that higher amounts of mineralisation were reported for the low seeding density (Mullen *et al*., 2013). Human marrow-derived MSC cells and MG-63 osteosarcoma cells encapsulated at low densities (2×10^6/3×10^6 cells/mL) within 3D collagen/alginate gels had higher ALP activity than cells seeded at higher densities (1×10^8/15×10^6 cells/mL) (Bitar *et al*., 2008; Maia *et al*., 2014). Here we showed that a low density (0.4×10^4 cells/cm^2 ~ 0.25×10^6 cells/mL) lead to higher ALP production after 3 d, compared to cells seeded at a high density (1.6×10^4 cells/cm^2 ~ 2×10^6 cells/mL). Furthermore, we observed an increase in calcium content in the high cell density (1.6×10^4 cells/cm^2 ~ 2×10^6 cells/mL) group within a low and high stiffness matrix compared to the other groups by 56 d.

The osteocyte network is analogous to the neuronal network, whereby neurons extend long interconnected dendrites. Studies have shown an increase in the percentage of neurons on 2D substrates (0.25-7 kPa) (Georges *et al*., 2006; Previtera *et al*., 2010), while in soft 3D agarose gels (~ 0.002 kPa) increased elongation rates of neurites relative to stiff gels (~ 0.13 kPa) have been observed (Balgude *et al*., 2001). Interestingly, DMP-1 expression has also been observed within the brain, suggesting strong ties with dendrite formation in neuron cells (Kalajzic *et al*., 2004). Therefore, we propose that the formation of a dendritic interconnected network within both neurons and osteocytes is driven by ECM stiffness and cell density.

Our results show that cells within a soft 3D matrix are dispersed throughout long-term culture and form interconnections with neighbouring cells (Fig. 4**A** & Fig. 5**A**), whereas those near the surface proliferate and form a confluent layer on the surface of the hydrogel, see Fig. 7. Similarly, HepG2 cells proliferate more when grown on 2D collagen substrates than when encapsulated within a 3D alginate gels (Lan *et al*., 2010). It is intriguing to speculate on the potential mechanisms by which embedded cells form dendrites and interconnected networks inside gelatin hydrogels. Our live cell results (Fig. 9**A**) and other studies (Balgude *et al*., 2001; Dallas *et al*., 2013; Dallas and Bonewald, 2010; Shahar and Dean, 2013; Webster *et al*., 2013) have shown that osteocytes and neurites are highly dynamic and repeatedly extend and retract their dendrites, and can establish connections with neighbouring cells through gap junctions (Doty, 1981; Palumbo *et al*., 2004) to form interconnected networks. Osteocyte dendrite formation is highly dependent on continuous cleavage of collagen through enzymes known as matrix metalloproteinases (MMPs) (Holmbeck *et al*., 2005), which are expressed by osteocytes (Hatori *et al*., 2004). Interestingly, matrix degradation through MMP activity has been shown in gelatin gels (d'Ortho *et al*., 1998). Therefore, we propose that osteoblastic cells encapsulated with softer matrices form dendrites and express MMPs to degrade the matrix macromolecules, allowing for the dendrite to perforate through the matrix. The higher degree of crosslinking between matrix macromolecules in the high stiffness group might present a matrix that is more difficult to degrade and thus explain the lower proportion of dendritic cells in these matrices.

The use of osteoblast-like MC3T3-E1 cell-line is a possible limitation of this study. However, isolating primary osteoblasts can produce inhomogeneous cell populations and osteoblast-specific features can be lost

upon subcultivation (Leis *et al*., 1997; Quarles *et al*., 1992). The MC3T3-E1 osteoblast cell line represents a uniformly defined cell population, which have similar traits to primary cells and can be readily expanded (Czekanska *et al*., 2012) and differentiated (Chatterjee *et al*., 2010; Keogh *et al*., 2010; Krishnan *et al*., 2010; Mullen *et al*., 2013; Partap *et al*., 2010; Przybylowski *et al*., 2012; St-Pierre *et al*., 2005; Uchihashi *et al*., 2013), making the cell line a good representative of pre-osteoblasts (Grigoriadis *et al*., 1985; Quarles *et al*., 1992; Sudo *et al*., 1983; Wang *et al*., 1999). It should be noted that ALP activity was only assessed from extracellular ALP in the media at specific time-points and thus might not be a reflection of the total ALP activity. Finally, we did not investigate precisely the mechanical environment that arises during osteocyte differentiation *in vivo* or the mechanical environment known to elicit osteoblast-osteocyte differentiation in 2D (~ 0.3 kPa) (Mullen *et al*., 2013). However, the mechanical properties of osteoid are unknown, as newly laid down osteoid tissue represents a thin layer approximately 350 nm deep, which has made the extraction of samples for mechanical testing unfeasible. Moreover, maintaining a homogeneous cell distribution in a low stiffness 3D matrix (~ 0.3 kPa) proved challenging as the cells settled at the bottom of the well before gelling occurred, whereas 0.58 kPa was found to be the lowest achievable matrix stiffness to avoid settling from occurring. Nonetheless the results of this study showed that osteocyte differentiation of MC3T3-E1 cells was indeed regulated within a 3D cell environment by ECM stiffness and cell density.

Various *in vitro* bone TE approaches, including porous biomaterial scaffolds (Correia *et al*., 2012; Curtin *et al*., 2012; Gleeson *et al*., 2010; Keogh *et al*., 2010), cellular aggregates (Freeman *et al*., 2015; Fuchs *et al*., 2007; Rouwkema *et al*., 2006) and cell encapsulation within hydrogels (Castillo Diaz *et al*., 2014; Chatterjee *et al*., 2010; Shin *et al*., 2014; Tan *et al*., 2014), have shown potential for bone regeneration, as indicated by osteogenic protein and mineral production. However, none of these have reported substantial osteocyte differentiation, dendrite formation or interconnected osteocyte networks within the constructs. The approach developed here may be a promising tool to reproduce bone constructs with an osteocyte network in place, which is an essential component in the formation of bone and the treatment of large bone defects.

Conclusion

The results of this study show that external biophysical and biochemical cues, such as matrix stiffness and cell density, control the phenotypic shift from osteoblasts to osteocytes in a 3D environment. For the first time MC3T3 - E1 osteoblast cells, at a seeding density of 2×10^6 cells/mL within a soft 3D matrix (0.58 kPa), have been induced to undergo osteocyte differentiation and form an interconnected network by 56 d of culture. On the matrix surface a confluent layer, representative of osteoblastic differentiation, was established. These results were achieved without the addition of growth factors. We propose that the encapsulation of cells within a soft matrix simulates the *in vivo* environment, wherein osteoblasts start to differentiate towards osteocytes after they have become embedded within osteoid, a soft unmineralised bone matrix. Future TE approaches could apply this method to develop bone constructs with an osteocyte network in place.

Acknowledgements

This project was supported by the European Research Council Grant 258992 (BONEMECHBIO). The authors acknowledge the facilities and scientific and technical assistance of the Centre for Microscopy & Imaging at the National University of Ireland Galway (www.imaging.nuigalway.ie), a facility that is funded by NUIG and the Irish Government's Programme for Research in Third Level Institutions, Cycles 4 and 5, National Development Plan 2007-2013.

References

Anderson EJ, Knothe Tate ML (2008) Idealization of pericellular fluid space geometry and dimension results in a profound underprediction of nano-microscale stresses imparted by fluid drag on osteocytes. J Biomech **41**: 1736-1746.

Atkins GJ, Welldon KJ, Wijenayaka AR, Bonewald LF, Findlay DM (2009) Vitamin K promotes mineralization, osteoblast-to-osteocyte transition, and an anticatabolic phenotype by {gamma}-carboxylation-dependent and -independent mechanisms. Am J Physiol Cell Physiol **297**: C1358-C1367.

Balgude AP, Yu X, Szymanski A, Bellamkonda RV (2001) Agarose gel stiffness determines rate of DRG neurite extension in 3D cultures. Biomaterials **22**: 1077-1084.

Barragan-Adjemian C, Nicolella D, Dusevich V, Dallas MR, Eick JD, Bonewald LF (2006) Mechanism by which MLO-A5 late osteoblasts/early osteocytes mineralize in culture: similarities with mineralization of lamellar bone. Calcif Tissue Int **79**: 340-353.

Bitar M, Brown RA, Salih V, Kidane AG, Knowles JC, Nazhat SN (2008) Effect of cell density on osteoblastic differentiation and matrix degradation of biomimetic dense collagen scaffolds. Biomacromolecules **9**: 129-135.

Boukhechba F, Balaguer T, Michiels JF, Ackermann K, Quincey D, Bouler JM, Pyerin W, Carle GF, Rochet N (2009) Human primary osteocyte differentiation in a 3D culture system. J Bone Miner Res **24**: 1927-1935.

Burger EH, Klein-Nulend J (1999) Mechanotransduction in bone-role of the lacuno-canalicular network. FASEB J **13**: S101-S112.

Castillo Diaz LA, Saiani A, Gough JE, Miller AF (2014) Human osteoblasts within soft peptide hydrogels promote mineralisation *in vitro*. J Tissue Eng **5**: doi: 10.1177/2041731414539344.

Chatterjee K, Lin-Gibson S, Wallace WE, Parekh SH, Lee YJ, Cicerone MT, Young MF, Simon CG JR (2010) The effect of 3D hydrogel scaffold modulus on

osteoblast differentiation and mineralization revealed by combinatorial screening. Biomaterials **31**: 5051-5062.

Correia C, Bhumiratana S, Yan LP, Oliveira AL, Gimble JM, Rockwood D, Kaplan DL, Sousa RA, Reis RL, Vunjak-Novakovic G (2012) Development of silk-based scaffolds for tissue engineering of bone from human adipose-derived stem cells. Acta Biomater **8**: 2483-2492.

Curtin CM, Cunniffe GM, Lyons FG, Bessho K, Dickson GR, Duffy GP, O'Brien FJ (2012) Innovative collagen nano-hydroxyapatite scaffolds offer a highly efficient non-viral gene delivery platform for stem cell-mediated bone formation. Adv Mater **24**: 749-754.

Czekanska EM, Stoddart MJ, Richards RG, Hayes JS (2012) In search of an osteoblast cell model for *in vitro* research. Eur Cell Mater **24**: 1-17.

d'Ortho MP, Stanton H, Butler M, Atkinson SJ, Murphy G, Hembry RM (1998) MT1-MMP on the cell surface causes focal degradation of gelatin films. FEBS Lett **421**: 159-164.

D'Souza RN, Cavender A, Sunavala G, Alvarez J, Ohshima T, Kulkarni AB, MacDougall M (1997) Gene expression patterns of murine dentin matrix protein 1 (Dmp1) and dentin sialophosphoprotein (DSPP) suggest distinct developmental functions *in vivo*. J Bone Miner Res **12**: 2040-2049.

Dallas SL, Bonewald LF (2010) Dynamics of the transition from osteoblast to osteocyte. Ann N Y Acad Sci **1192**: 437-443.

Dallas SL, Prideaux M, Bonewald LF (2013) The osteocyte: an endocrine cell and more. Endocr Rev **34:** 658-690.

Doty SB (1981) Morphological evidence of gap junctions between bone cells. Calcif Tissue Int **33**: 509-512.

Engler A, Bacakova L, Newman C, Hategan A, Griffin M, Discher D (2004) Substrate compliance *versus* ligand density in cell on gel responses. Biophys J **86**: 617-628.

Engler AJ, Sen S, Sweeney HL, Discher DE (2006) Matrix elasticity directs stem cell lineage specification. Cell **126**: 677-689.

Evans ND, Minelli C, Gentleman E, LaPointe V, Patankar SN, Kallivretaki M, Chen X, Roberts CJ, Stevens MM (2009) Substrate stiffness affects early differentiation events in embryonic stem cells. Eur Cell Mater **18**: 1-13.

Feng JQ, Zhang J, Dallas SL, Lu Y, Chen S, Tan X, Owen M, Harris SE, MacDougall M (2002) Dentin matrix protein 1, a target molecule for Cbfa1 in bone, is a unique bone marker gene. J Bone Miner Res **17**: 1822-1831.

Freeman FE, Haugh MG, McNamara LM (2015) An *in vitro* bone tissue regeneration strategy combining chondrogenic and vascular priming enhances the mineralization potential of mesenchymal stem cells *in vitro* while also allowing for vessel formation. Tissue Eng Part A **21**: 1320-1332.

Fuchs S, Hofmann A, Kirkpatrick C (2007) Microvessel-like structures from outgrowth endothelial cells from human peripheral blood in 2-dimensional and 3-dimensional co-cultures with osteoblastic lineage cells. Tissue Eng **13**: 2577-2588.

Georges PC, Miller WJ, Meaney DF, Sawyer ES, Janmey PA (2006) Matrices with compliance comparable to that of brain tissue select neuronal over glial growth in mixed cortical cultures. Biophys J **90**: 3012-3018.

Gleeson JP, Plunkett NA, O'Brien FJ (2010) Addition of hydroxyapatite improves stiffness, interconnectivity and osteogenic potential of a highly porous collagen-based scaffold for bone tissue regeneration. Eur Cell Mater **20**: 218-230.

Grigoriadis AE, Petkovich PM, Ber R, Aubin JE, Heersche JN (1985) Subclone heterogeneity in a clonally-derived osteoblast-like cell line. Bone **6**: 249-256.

Hadjipanayi E, Mudera V, Brown RA (2009) Close dependence of fibroblast proliferation on collagen scaffold matrix stiffness. J Tissue Eng Regen Med **3**: 77-84.

Han Y, Cowin SC, Schaffler MB, Weinbaum S (2004) Mechanotransduction and strain amplification in osteocyte cell processes. Proc Natl Acad Sci U S A **101**: 16689-16694.

Harley BA, Leung JH, Silva EC, Gibson LJ (2007) Mechanical characterization of collagen-glycosaminoglycan scaffolds. Acta Biomater **3**: 463-474.

Hatori K, Sasano Y, Takahashi I, Kamakura S, Kagayama M, Sasaki K (2004) Osteoblasts and osteocytes express MMP2 and -8 and TIMP1, -2, and -3 along with extracellular matrix molecules during appositional bone formation. Anat Rec A Discov Mol Cell Evol Biol **277**: 262-271.

Haugh MG, Murphy CM, McKiernan RC, Altenbuchner C, O'Brien FJ (2011) Crosslinking and mechanical properties significantly influence cell attachment, proliferation, and migration within collagen glycosaminoglycan scaffolds. Tissue Eng Part A **17**: 1201-1208.

Holmbeck K, Bianco P, Pidoux I, Inoue S, Billinghurst RC, Wu W, Chrysovergis K, Yamada S, Birkedal-Hansen H, Poole AR (2005) The metalloproteinase MT1-MMP is required for normal development and maintenance of osteocyte processes in bone. J cell Sci **118**: 147-156

Huebsch N, Arany PR, Mao AS, Shvartsman D, Ali OA, Bencherif SA, Rivera-Feliciano J, Mooney DJ (2010) Harnessing traction-mediated manipulation of the cell/matrix interface to control stem-cell fate. Nat Mater **9**: 518-526.

Jee WS (2001) Integrated Bone Tissue Physiology. In Bone Mech. Handbook, Second Ed., 1-68. CRC Press, March 15. doi:10.1201/b14263-3.

Kalajzic I, Braut A, Guo D, Jiang X, Kronenberg MS, Mina M, Harris MA, Harris SE, Rowe DW (2004) Dentin matrix protein 1 expression during osteoblastic differentiation, generation of an osteocyte GFP-transgene. Bone **35**: 74-82.

Keogh MB, O'Brien FJ, Daly JS (2010) Substrate stiffness and contractile behaviour modulate the functional maturation of osteoblasts on a collagen-GAG scaffold. Acta Biomater **6**: 4305-4313.

Kim K, Dean D, Mikos AG, Fisher JP (2009) Effect of initial cell seeding density on early osteogenic signal expression of rat bone marrow stromal cells cultured on cross-linked poly(propylene fumarate) disks. Biomacromolecules **10**: 1810-1817.

Knothe Tate ML, Steck R, Forwood MR, Niederer P (2000) *In vivo* demonstration of load-induced fluid flow

in the rat tibia and its potential implications for processes associated with functional adaptation. J Exp Biol **203**: 2737-2745.

Knothe Tate ML, Niederer P, Knothe U (1998) *In vivo* tracer transport through the lacunocanalicular system of rat bone in an environment devoid of mechanical loading. Bone **22**: 107-117.

Knothe Tate ML, Adamson JR, Tami AE, Bauer TW (2004) The osteocyte. Int J Biochem Cell Biol **36**: 1-8.

Knothe Tate ML, Niederer P (1998) Theoretical FE-based model developed to predict the relative contribution of convective and diffusive transport mechanisms for the maintenance of local equilibria within cortical bone. In Pap. Present. ASME Heat Transfer Div Publ HTD **362:** 133-141.

Krishnan V, Dhurjati R, Vogler EA, Mastro AM (2010) Osteogenesis *in vitro*: from pre-osteoblasts to osteocytes: a contributuion from the Osteobiology Research Group, The Pennsylvania State University. In Vitro Cell Dev Biol Anim **46**: 28-35.

Lan SF, Safiejko-Mroczka B, Starly B (2010) Long-term cultivation of HepG2 liver cells encapsulated in alginate hydrogels: a study of cell viability, morphology and drug metabolism. Toxicol In Vitro **24**: 1314-1323.

Lee JW, Yamaguchi A, Iimura T (2014) Functional heterogeneity of osteocytes in FGF23 production: the possible involvement of DMP1 as a direct negative regulator. Bonekey Rep **3**: 543.

Legant WR, Miller JS, Blakely BL, Cohen DM, Genin GM, Chen CS (2010) Measurement of mechanical tractions exerted by cells in three-dimensional matrices. Nat Methods **7**: 969-971.

Leis HJ, Hulla W, Gruber R, Huber E, Zach D, Gleispach H, Windischhofer W (1997) Phenotypic heterogeneity of osteoblast-like MC3T3-E1 cells: changes of bradykinin-induced prostaglandin E2 production during osteoblast maturation. J Bone Miner Res **12**: 541-551.

Lo CM, Wang HB, Dembo M, Wang YL (2000) Cell movement is guided by the rigidity of the substrate. Biophys J **79**: 144-152.

Maia FR, Lourenço AH, Granja PL, Gonçalves RM, Barrias CC (2014) Effect of cell density on mesenchymal stem cells aggregation in RGD-alginate 3D matrices under osteoinductive conditions. Macromol Biosci **14**: 759-771.

McNamara LM, Majeska RJ, Weinbaum S, Friedrich V, Schaffler MB (2009) Attachment of osteocyte cell processes to the bone matrix. Anat Rec (Hoboken). **292**: 355-363.

Mikuni-Takagaki Y, Kakai Y, Satoyoshi M, Kawano E, Suzuki Y, Kawase T, Saito S (1995) Matrix mineralization and the differentiation of osteocyte-like cells in culture. J Bone Miner Res **10**: 231-242.

Mullen CA, Haugh MG, Schaffler MB, Majeska RJ, McNamara LM (2013) Osteocyte differentiation is regulated by extracellular matrix stiffness and intercellular separation. J Mech Behav Biomed Mater **28**: 183-194.

Mullen CA, Vaughan TJ, Voisin MC, Brennan MA, Layrolle P, McNamara LM (2014) Cell morphology and focal adhesion location alters internal cell stress. J R Soc Interface **11**:. doi: 10.1098/rsif.2014.0885.

Murshid SA, Kamioka H, Ishihara Y, Ando R, Sugawara Y, Takano-Yamamoto T (2007) Actin and microtubule cytoskeletons of the processes of 3D-cultured MC3T3-E1 cells and osteocytes. J Bone Miner Metab **25**: 151-158.

Nakano Y, Beertsen W, Van Den Bos T, Kawamoto T, Oda K, Takano Y (2004) Site-specific localization of two distinct phosphatases along the osteoblast plasma membrane: tissue non-specific alkaline phosphatase and plasma membrane calcium ATPase. Bone **35**: 1077-1085.

Narayanan K, Ramachandran A, Hao J, He G, Park KW, Cho M, George A (2003) Dual functional roles of dentin matrix protein 1. Implications in biomineralization and gene transcription by activation of intracellular Ca2+ store. J Biol Chem **278**: 17500-17508.

Palazzini S, Palumbo C, Ferretti M, Marotti G (1998) Stromal cell structure and relationships in perimedullary spaces of chick embryo shaft bones. Anat Embryol (Berl) **197**: 349-357.

Palumbo C (1986) A three-dimensional ultrastructural study of osteoid-osteocytes in the tibia of chick embryos. Cell Tissue Res **246**: 125-131.

Palumbo C, Ferretti M, Marotti G (2004) Osteocyte dendrogenesis in static and dynamic bone formation: an ultrastructural study. Anat Rec A Discov Mol Cell Evol Biol **278**: 474-480.

Partap S, Plunkett NA, Kelly DJ, O'Brien FJ (2010) Stimulation of osteoblasts using rest periods during bioreactor culture on collagen-glycosaminoglycan scaffolds. J Mater Sci Mater Med **21**: 2325-2330.

Previtera ML, Langhammer CG, Firestein BL (2010) Effects of substrate stiffness and cell density on primary hippocampal cultures. J Biosci Bioeng **110**: 459-470.

Prideaux M, Loveridge N, Pitsillides AA, Farquharson C (2012) Extracellular matrix mineralization promotes E11/gp38 glycoprotein expression and drives osteocytic differentiation. **PLoS One 7:** e36786.

Przybylowski C, Quinn T, Callahan A, Kaplan M, Golding A, Alesi C, Ammar M, LeBlon CE, Guo Y, Zhang X, Jedlicka SS (2012) MC3T3 preosteoblast differentiation on bone morphogenetic protein-2 peptide ormosils. J Mater Chem **22**: 10672-10683.

Quarles LD, Yohay DA, Lever LW, Caton R, Wenstrup RJ (1992) Distinct proliferative and differentiated stages of murine MC3T3-E1 cells in culture: an *in vitro* model of osteoblast development. J Bone Miner Res **7**: 683-692.

Rios HF, Ye L, Dusevich V, Eick D, Bonewald LF, Feng JQ (2005) DMP1 is essential for osteocyte formation and function. J Musculoskelet Neuronal Interact **5**: 325-327.

Rouwkema J, de Boer J, Van Blitterswijk CA (2006) Endothelial cells assemble into a 3-dimensional prevascular network in a bone tissue engineering construct. Tissue Eng **12**: 2685-2693.

Shahar R, Dean MN (2013) The enigmas of bone without osteocytes. Bonekey Rep **2**: 343.

Shin H, Olsen BD, Khademhosseini A (2014) Gellan gum microgel-reinforced cell-laden gelatin hydrogels. J Mater Chem B Mater Biol Med **2**: 2508-2516.

Soares CP, Midlej V, de Oliveira ME, Benchimol M, Costa ML, Mermelstein C (2012) 2D and 3D-organized cardiac cells shows differences in cellular morphology, adhesion junctions, presence of myofibrils and protein

expression. **PLoS One 7:** doi:10.1371/journal.pone.0038147.

St-Pierre JP, Gauthier M, Lefebvre L-P, Tabrizian M (2005) Three-dimensional growth of differentiating MC3T3-E1 pre-osteoblasts on porous titanium scaffolds. Biomaterials **26**: 7319-7328.

Sudo H, Kodama HA, Amagai Y, Yamamoto S, Kasai S (1983) *In vitro* differentiation and calcification in a new clonal osteogenic cell line derived from newborn mouse calvaria. J Cell Biol **96**: 191-198.

Tan S, Fang JY, Yang Z, Nimni ME, Han B (2014) The synergetic effect of hydrogel stiffness and growth factor on osteogenic differentiation. Biomaterials **35**: 5294-5306.

Uchihashi K, Aoki S, Matsunobu A, Toda S (2013) Osteoblast migration into type I collagen gel and differentiation to osteocyte-like cells within a self-produced mineralized matrix: a novel system for analyzing differentiation from osteoblast to osteocyte. Bone **52**: 102-110.

Verbruggen SW, Vaughan TJ, McNamara LM (2012) Strain amplification in bone mechanobiology: a computational investigation of the *in vivo* mechanics of osteocytes. J R Soc Interface **9**: 2735-2744.

Wang D, Christensen K, Chawla K, Xiao G, Krebsbach PH, Franceschi RT (1999) Isolation and characterization of MC3T3-E1 preosteoblast subclones with distinct *in vitro* and *in vivo* differentiation/mineralization potential. J Bone Miner Res **14**: 893-903.

Wang LS, Du C, Chung JE, Kurisawa M (2012) Enzymatically cross-linked gelatin-phenol hydrogels with a broader stiffness range for osteogenic differentiation of human mesenchymal stem cells. Acta Biomater **8**: 1826-1837.

Wang L, Cowin SC, Weinbaum S, Fritton SP (2000) Modeling tracer transport in an osteon under cyclic loading. Ann Biomed Eng **28**: 1200-1209.

Wang L, Wang Y, Han Y, Henderson SC, Majeska RJ, Weinbaum S, Schaffler MB (2005) *In situ* measurement of solute transport in the bone lacunar-canalicular system. Proc Natl Acad Sci USA **102**: 11911-11916.

Wang Y, McNamara LM, Schaffler MB, Weinbaum S (2007) A model for the role of integrins in flow induced mechanotransduction in osteocytes. Proc Natl Acad Sci **104**: 15941-15946.

Webster DJ, Schneider P, Dallas SL, Müller R (2013) Studying osteocytes within their environment. Bone **54**: 285-295.

Weinbaum S, Cowin SC, Zeng Y (1994) A model for the excitation of osteocytes by mechanical loading-induced bone fluid shear stresses. J Biomech **27**: 339-360.

Woo SM, Rosser J, Dusevich V, Kalajzic I, Bonewald LF (2011) Cell line IDG-SW3 replicates osteoblast-to-late-osteocyte differentiation *in vitro* and accelerates bone formation *in vivo.* J Bone Miner Res **26**: 2634-2646.

You L, Cowin SC, Schaffler MB, Weinbaum S (2001) A model for strain amplification in the actin cytoskeleton of osteocytes due to fluid drag on pericellular matrix. J Biomech **34**: 1375-1386.

Zaman MH, Trapani LM (2006) Migration of tumor cells in 3D matrices is governed by matrix stiffness along with cell-matrix adhesion and proteolysis. Proc Natl Acad Sci USA **103**: 10889-10894.

Zeng Y, Cowin SC, Weinbaum S (1994) A fiber-matrix model for fluid-flow and streaming potentials in the canaliculi of an osteon. Ann Biomed Eng **22**: 280-292.

Zhang K, Barragan-Adjemian C, Ye L, Kotha S, Dallas M, Lu Y, Zhao S, Harris M, Harris SE, Feng JQ, Bonewald LF (2006) E11/gp38 selective expression in osteocytes: regulation by mechanical strain and role in dendrite elongation. Mol Cell Biol **26**: 4539-4552.

Zhou H, Weir MD, Xu HH (2011) Effect of cell seeding density on proliferation and osteodifferentiation of umbilical cord stem cells on calcium phosphate cement-fiber scaffold. Tissue Eng Part A **17**: 2603-2613.

Discussion with Reviewer

Reviewer I: In your previous work, evaluating the effect of cell density and material stiffness on osteocyte differentiation in 2D (Mullen *et al.,* 2013), the authors showed that low cell density favoured osteocyte differentiation, while high cell density preserved osteoblast phenotype. Could the authors speculate why different results were achieved within the current manuscript evaluating osteocyte differentiation in 3D?

Authors: In our previous work (Mullen *et al.,* 2013) we studied cells seeded on a flat 2D surface at a low initial cell density of 1,000 cells/cm^2. The cells were shown to maintain a low cell density for the 14 d experiment. We proposed that the initial low cell density and the mechanics of the substrate together prevented cells from proliferating sufficiently and after a time resorted to extending processes to establish a communication network with neighbouring cells. However, in our 3D environment 2 million cells were initially encapsulated in a 1 cm^3 volume of gelatin-mtgase matrix. If all cells were successfully encapsulated and remained viable, we would expect an initially high cell density of approximately 16,000 cells/cm^2. However, we did observe that approximately 80 % of cells were "dormant" at day 21 in the soft matrix stiffness at the high cell density group (data not shown), showing no normal cell activity (dendritic, motile, change in cell morphology, *etc.)* throughout the culture period, and these were excluded from further analysis. Therefore, the active population of osteoblasts/osteocytes might be closer to 3,200 cells/cm^2. Moreover, in the 3D environment the cells are confined on all sides by the gelatin-mtgase matrix, limiting the differentiation into osteocytes as the cells need to degrade the surrounding matrix to create space for dendrites. Thus, it is not possible to fully compare the cell densities between the 2D and 3D environments. However, the different results achieved within the current manuscript, *i.e.* high initial cell density favoured osteocyte differentiation, are likely explained due to a combination of the large population of inactive cells and the presentation of a 3D mechanical environment during cell encapsulation, which will place further spatial constraints on the extension of dendrites. Other studies have shown that cell encapsulation within a 3D matrix can prevent proliferation in cell types such

as, cardiac cells, human embryonic stem cells and HepG2 liver cells (Lan *et al.,* 2010; Soares *et al.,* 2012; Tian *et al.,* 2008).

Reviewer I: Did the authors see the formation of a surface-cell-layer already earlier than day 56? Could you speculate on the formation of this layer – de-differentation of cells, or just migration and subsequent cell proliferation?
Authors: A low confluency surface layer of cells was observed by approximately 20-30 d in the high cell density groups, whereas in the other cell density groups the surface layer formed at approximately 30-40 d. The surface layer of cells was not present at earlier time-points; however, a homogenous distribution of cells was observed throughout the hydrogel including cells encapsulated near the surface of the hydrogel after fabrication. Based on these observations, the authors propose that cells near the surface migrated out of the hydrogel and then started to proliferate at the surface, forming a confluent layer over the rest of the culture period.

Reviewer I: The authors report increased mineralisation in the high-cell-density group. Would the authors suspect an increase in matrix stiffness in this group that is superior over the other groups?
Authors: Mineral concentration is a key determinant of the mechanical properties of bone (Currey, 1984; Ruffoni *et al.,* 2007). Increase in matrix stiffness due to mineralisation has been observed in silk scaffolds seeded with human bone marrow stem cells (Kim *et al.,* 2007), polyurethane scaffolds seeded with MLO-A5 osteoblastic cells (Sittichockechaiwut *et al.,* 2009) and also in peptide hydrogels containing encapsulated human osteoblasts cells (Castillo Diaz *et al.,* 2014). Thus the authors would expect an increase in matrix stiffness compared to the other cell density groups at that stiffness.

Reviewer I: Could the authors speculate on the role of matrix stiffening during late osteocyte differentiation?
Authors: Osteocyte differentiation and matrix stiffness are inextricably linked. *In vivo*, osteoblasts primarily lay down a soft collagen matrix known as osteoid, onto which mineral crystals are subsequently deposited (Barragan-Adjemian *et al.,* 2006). However, there is a mineralisation lag time, which allows for osteoblasts to become embedded in the soft collagen matrix. During this time the osteoblasts transition into early stage osteocytes. Both osteoblasts on the surface and differentiating osteocytes release phosphate ions, which in turn results in mineral crystal growth and will hence the increase in matrix stiffness (Barragan-Adjemian *et al.,* 2006). The stiff calcified osteoid acts a mediator of mechanical stimulation to the osteocyte through load induced fluid flow and cell-ECM interactions within the lacunar-canalicular system (McNamara *et al.,* 2009; Wang *et al.,* 2007). Studies have shown changes in gene expression that coincide with mineralisation. Increased levels of early osteocyte markers, such as E11/gp38/podoplanin and dentin matrix protein 1 are expressed after the cell becomes embedded within the soft matrix and continues to increase with mineralisation along with sclerostin, a marker of the mature osteocyte, expressed when the cell is completely surrounded by dense calcified matrix (Bonewald, 2011; Dallas *et al.,* 2013). It is intriguing to postulate that the development of a stiff matrix around the osteocyte and the ensuing change in mechanical stimulation would facilitate the terminal differentiation of the early stage osteocyte into an interconnected osteocyte that is mechanosensitive to its surrounding environment. However, as the change in matrix stiffness is itself caused by osteocyte differentiation future studies would be required to fully delineate the cause-effect relationships.

Additional References

Bonewald LF (2011) The amazing osteocyte. J Bone Miner Res **26:** 229-238.

Currey JD (1984) Effects of differences in mineralization on the mechanical properties of bone. Philos Trans R Soc Lond B Biol Sci **304:** 509-518.

Kim HJ, Kim UJ, Leisk GG, Bayan C, Georgakoudi I, Kaplan DL (2007) Bone regeneration on macroporous aqueous-derived silk 3-D scaffolds. Macromol Biosci **7:** 643-655.

Ruffoni D, Fratzl P, Roschger P, Klaushofer K, Weinkamer R (2007) The bone mineralization density distribution as a fingerprint of the mineralization process. Bone **40:** 1308-1319.

Sittichockechaiwut A, Scutt AM, Ryan AJ, Bonewald LF, Reilly GC (2009) Use of rapidly mineralising osteoblasts and short periods of mechanical loading to accelerate matrix maturation in 3D scaffolds. Bone **44:** 822-829.

Tian XF, Heng BC, Ge Z, Lu K, Rufaihah AJ, Fan VT, Yeo JF, Cao T (2008) Comparison of osteogenesis of human embryonic stem cells within 2D and 3D culture systems. Scand J Clin Lab Invest **68:** 58-67.

Editor‘s Note: Scientific Editor in charge of the paper: Martin Stoddart.